CASL-U-2015-0146-001

ORNL/SR-2015/640

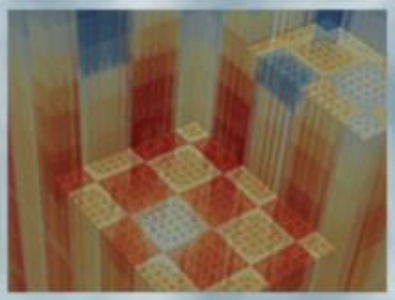

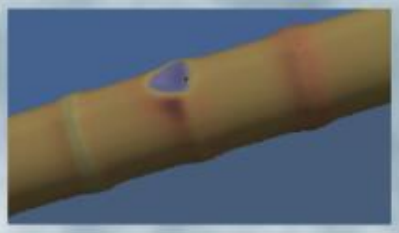

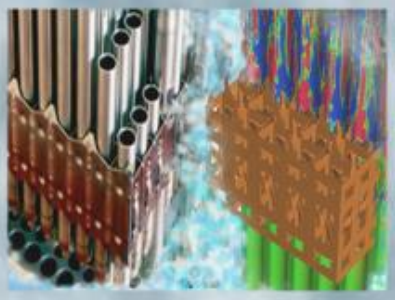

Coupling of Subchannel T/H (CTF) and CRUD Chemistry (MAMBA1D)

Robert Salko, Oak Ridge National Laboratory
Scott Palmtag, Core Physics
Benjamin Collins, Oak Ridge National Laboratory
Brian Kendrick, Los Alamos National Laboratory
Jeff Secker, Westinghouse Electric Company

05/15/2015

REVISION LOG

Revision	Date	Affected Pages	Revision Description
0	05/15/15	All	Initial Release
1	11/02/15	All	Updating results and responding to reviewer feedback

Document pages that are:

Export Controlled _____None_____

IP/Proprietary/NDA Controlled__None_____

Sensitive Controlled_____None_____

All pages marked for unlimited release

Requested Distribution:

To:

Copy: Jeff Banta

EXECUTIVE SUMMARY

The purpose of this milestone is to create a preliminary capability for modeling light water reactor (LWR) thermal-hydraulic (T/H) and CRUD growth using the CTF subchannel code and the subgrid version of the MAMBA CRUD chemistry code, MAMBA1D. In part, this is a follow-on to Milestone L3.PHI.VCS.P9.01, which is documented in Report CASL-U-2014-0188-000, titled "Development of CTF Capability for Modeling Reactor Operating Cycles with Crud Growth". As the title suggests, the previous milestone set up a framework for modeling reactor operation cycles with CTF. The framework also facilitated coupling to a CRUD chemistry capability for modeling CRUD growth throughout the reactor operating cycle. To demonstrate the capability, a simple CRUD "surrogate" tool was developed and coupled to CTF; however, it was noted that CRUD growth predictions by the surrogate were not considered realistic. This milestone builds on L3.PHI.VCS.P9.01 by replacing this simple surrogate tool with the more advanced MAMBA1D CRUD chemistry code. Completing this task involves addressing unresolved tasks from Milestone L3.PHI.VCS.P9.01, setting up an interface to MAMBA1D, and extracting new T/H information from CTF that was not previously required in the simple surrogate tool.

Specific challenges encountered during this milestone include (1) treatment of the CRUD erosion model, which requires local turbulent kinetic energy (TKE) (a value that CTF does not calculate) and (2) treatment of the MAMBA1D CRUD chimney boiling model in the CTF rod heat transfer solution. To demonstrate this new T/H, CRUD modeling capability, two sets of simulations were performed: (1) an 18 month cycle simulation of a quarter symmetry model of Watts Bar and (2) a simulation of Assemblies G69 and G70 from Seabrook Cycle 5. The Watts Bar simulation is merely a demonstration of the capability. The simulation of the Seabrook cycle, which had experienced CRUD-related fuel rod failures, had actual CRUD-scrape data to compare with results. As results show, the initial CTF/MAMBA1D-predicted CRUD thicknesses were about half of their expected values, so further investigation will be required for this simulation.

CONTENTS

FIGURES

TABLES

ACRONYMS

1D one-dimensional

2D two-dimensional

3D three-dimensional

CILC CRUD-induced localized corrosion

CIPS CRUD-induced power shift

LWR light water reactor

PWR pressurized water reactor

T/H thermal-hydraulic

TKE turbulent kinetic energy

1 INTRODUCTION

One of the primary CASL challenge problems is to better understand the effects of CRUD in the light water reactor (LWR), which includes modeling of CRUD-induced power shift (CIPS) and CRUD-induced localized corrosion (CILC). Meeting this challenge requires more advanced simulation tools capable of accurately modeling CRUD dynamics in the LWR environment. This milestone supports the CRUD challenge problem through the development of a preliminary multi-physics (thermal-hydraulic (T/H) and CRUD) analysis tool using the subchannel code, CTF, and the subgrid version of the advanced CRUD chemistry tool, MAMBA1D.

Figure 1 demonstrates the need for a multi-physics approach to modeling LWR CRUD growth. CRUD deposition is strongly driven by the strength and location of core boiling, which leads to coolant impurities depositing on fuel rod surfaces. Boiling is a function of rod surface temperature, coolant pressure, rod heat flux, and coolant temperature. Not only can local T/H conditions cause the growth of CRUD, but also they can cause its erosion. In this coupling, MAMBA1D obtains all of this information from the CTF solution.

The presence of the CRUD layer also impacts the T/H solution, as the CRUD deposits offer additional thermal resistance that increases internal rod temperatures. Furthermore, the boiling process changes from subcooled boiling on a clean rod surface to a combination of rod surface and CRUD chimney boiling, which impacts rod-to-fluid heat transfer. The coupling discussed in this paper covers these interactions.

The presence of CRUD does not just impact the T/H solution; its feedback on the neutronics behavior of the core is also important because the boron present in the CRUD layer acts as a local neutron absorber and can substantially change the shape of the core power distribution, leading to CIPS in severe cases. Because of this, future work will seek to expand this multi-physics package to a three-part coupling between MPACT, CTF, and MAMBA1D. This milestone is one part in a progression of milestones, which include

- L3.PHI.VCS.P9.01—Initial integration of CRUD code into CTF [1]
- L3.PHI.CTF.P10.02—Incorporation of MAMBA1D into CTF [2]
- L3:PHI.VCS.P11.01—CRUD coupling to MPACT [3]
- L2:PHI.P11.01—VERA-CS with CIPS Modeling Capability [4]
- L1:CASL.P11.03—Qualifying a core-wide PWR CIPS capability that includes an initial corrosion product treatment [5]

Completion of this milestone involves a collection of subtasks, each of which is detailed in the following sections of this report. This milestone is partly a follow-on to L3.PHI.VCS.P9.01 [1], which prepares CTF for coupling to a CRUD capability. At the time, the MAMBA1D source code was not available, so a simple CRUD surrogate was used in its place to create the infrastructure needed to do the coupling. This milestone both refines and extends the T/H-CRUD coupling work.

First, a brief introduction of the subgrid version of MAMBA1D is given in Section 2. Next, follow-on work from L3.PHI.VCS.P9.01 is discussed in Section 3.

The next task involves revisiting the coupling algorithm. Previously, the CRUD tool was not considering a time-averaged T/H profile when growing the CRUD; furthermore, no additional T/H iteration was being performed to update the internal rod temperature profiles to account for increased thermal resistance due to the CRUD layer. These issues are addressed by revising the coupling algorithm, which is documented in Section 4.

It is necessary to incorporate the MAMBA1D source from an infrastructure perspective (i.e., to link to the MAMBA1D source during the build of CTF). This is discussed in Section 5.

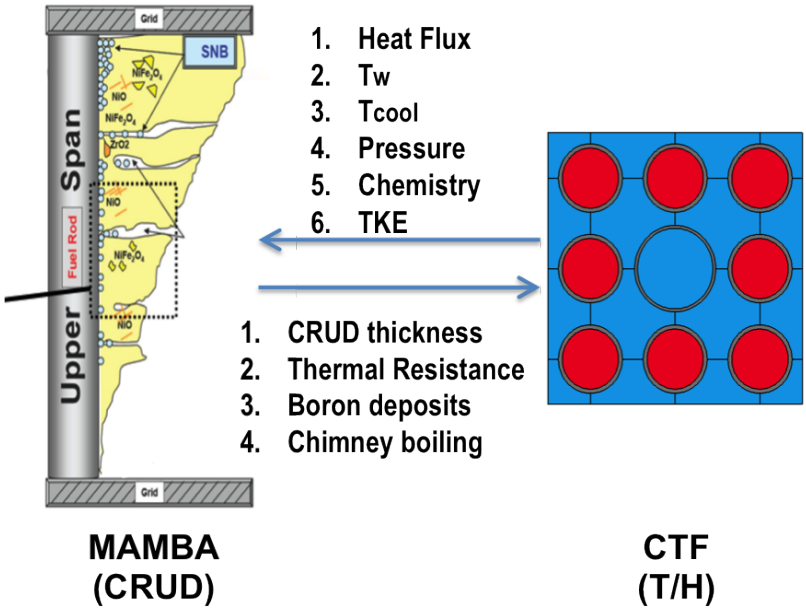

Figure 1. Data transfers considered in the developed coupled T/H, CRUD multi-physics package.

It has been noted that work is needed to collect additional data required by MAMBA1D that is not required of the surrogate. Some of this data, like wall temperature and heat flux, is a simple matter to collect; however, other data like the turbulent kinetic energy (TKE) presents a challenge. Section 6 discusses how TKE is calculated in CTF for use in the MAMBA1D CRUD erosion model.

The treatment of CRUD chimney boiling is another challenge to consider. MAMBA1D has its own model that predicts boiling (mass transfer and CRUD-to-coolant heat transfer) in the CRUD layer. CTF has its own model that is aimed at predicting surface subcooled and nucleate boiling. Therefore, it is necessary to consider how these models should be used in combination. Section 7 provides a discussion of the theory of the MAMBA1D boiling model and considers how the CTF and MAMBA1D models might be combined in the coupling.

Finally, after the coupling of CTF and MAMBA1D is completed, feature testing was required. This was achieved with a demonstration of modeling Watts Bar Unit 1 at quarter symmetry with a realistic CTF/MPACT coupled power distribution over an 18 month operating cycle. Although this study is more of a demonstration, a more realistic simulation is performed on the Seabrook Cycle 5 simulation. Section 8 presents the results of these simulations.

2 MAMBA1D CRUD Chemistry Code

MAMBA1D uses a pragmatic multi-scale approach to address the physics and chemistry of CRUD formation and growth and subsequent impact on CIPS and CILC. Microscale models provide detailed temperature and species distributions in the CRUD layer. Engineering-scale models take averaged microscale distributions as input and determine CRUD thickness, porosity, and composition. The MAMBA1D code has three-dimensional (3D) and two-dimensional (2D). In preparation for this work and for a previous coupling with Hydra-TH, a subgrid version of the code, complete with a coupling interface for T/H codes, was developed as part of Milestone L3:THM.CFD.P9.11.

The subgrid version differs from its 2-D and 3-D counterparts in that it "meshes" the CRUD layer in the radial direction only. There is no heat transfer or variation in CRUD thickness or composition in the azimuthal or axial directions for a single instance of MAMBA1D. However, it is important to note that this subgrid version is intended to be called many times over the surface of a single fuel rod so that the CRUD geometry and composition will still respond to localized T/H effects.

MAMBA1D solves a one-dimensional (1D) conduction equation for this radial mesh. The boundary conditions include CRUD surface temperature and clad heat flux, both of which are supplied by calling the T/H code. MAMBA1D also includes a boiling model that acts as a heat sink in the conduction equation solution. Using the boiling model and coolant chemistry information that is passed through the coupling interface, the code determines where and how compounds like boron, lithium, iron, and nickel deposit on the rod surface.

CRUD is grown over an amount of time specified by the coupled T/H code. Upon completion of the solution, MAMBA1D returns information of interest to the T/H code, which includes CRUD layer thermal resistance, chimney boiling rate, and CRUD composition.

3 L3.PHI.VCS.P9.02 Follow-Up

Document number CASL-U-2014-0188-000 noted that work was needed to better organize CRUD-related data and procedures and that multistate driver access to CTF internal data should be eliminated. This was needed as, ultimately, other codes that do not reside in the CTF repository (i.e., MPACT), will be used to drive the coupling in place of the multistate driver and will not have access to CTF internal data. Rather, the CRUD modeling should be entirely controllable through a small set of straightforward procedures in the CTF Coupling Interface. Furthermore, work was needed to collect additional data needed by MAMBA1D that the surrogate did not require.

3.1 CrudLayer Class

Initially, the multistate driver was designed to loop over all rod surfaces in the CTF model and directly call the CRUD-modeling surrogate. This required the multistate driver to know about the geometry in CTF (e.g., number of rods, surfaces per rods, number of levels) and the operating conditions (e.g., rod surface boiling rates, heat flux) for inputting into the surrogate. Since the multistate driver was developed to be an external driver of CTF, it made more sense to remove all of this cross-contamination of data and, instead, have the multistate driver call a procedure in the CTF Coupling Interface that takes care of growing the CRUD on all fuel rods for a given state.

This is done by adding a procedure called "CTF_grow_crud" to the CTF Coupling Interface module. The procedure for growing the CRUD has to loop over all rods, gather internal CTF data needed by both the surrogate and MAMBA1D, and then call either the surrogate or MAMBA1D for each rod surface. In addition to these actions, a place is needed to house CRUD-related data, which includes thermal resistance, CRUD thickness, and new MAMBA1D-related data. To meet this requirement with proper organization in mind, a new class is created in CTF called the "CrudLayer" class. This class has a relationship with the "FuelRod" and "Surface" classes in CTF that is defined by the UML diagram in Figure 2.

The FuelRod class physically represents a solid conductor in the CTF model; it may be a wall, a tube, or a nuclear fuel rod. As seen in the diagram, the FuelRod class contains an array of Surface objects. Physically, a Surface object is a connection between a rod and a channel; a Surface type houses data like heat flux, heat transfer coefficients, and surface temperature. In square rod lattice geometry (like that of an LWR), a fuel rod will connect to four channels and, therefore, the "surf" array in the FuelRod class will be size four. In other words, a FuelRod will have four Surface objects.

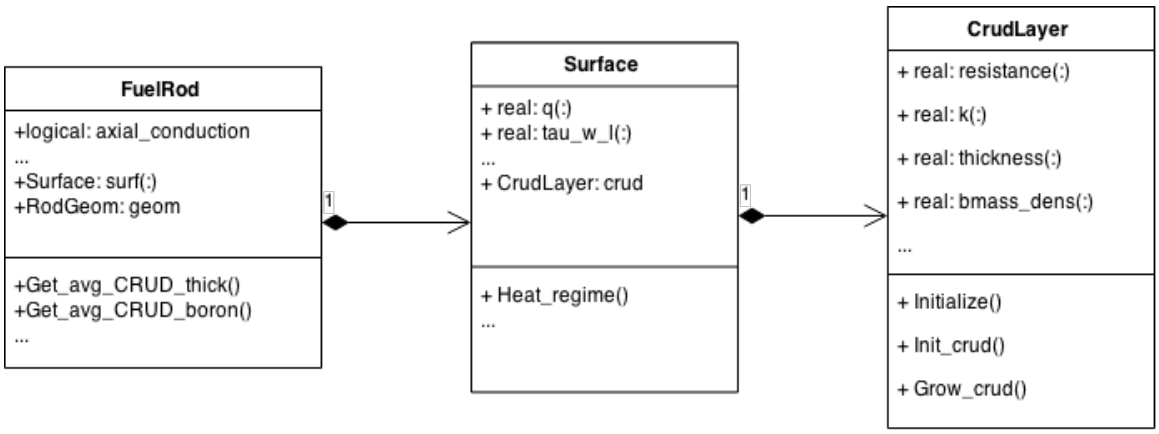

Figure 2. UML diagram for the FuelRod, Surface, and CrudLayer classes in CTF.

Note that both FuelRod and Surface types have an axial component. In other words, the fuel rod in CTF is discretized in the axial direction. This means that surface data is stored in 1-D vectors, where the vector takes an axial index identification that points to a certain axial level of the rod. The axial meshing of the FuelRod and Surface is, of course, conformal. This concept of fuel rods and surfaces is further illustrated by Figure 3, which shows a single fuel rod that connects to four channels. Because the rod connects to four channels, it will have four azimuthal segments and, thus, four surfaces. A single surface is highlighted in red. The surface extends from the bottom to the top of the rod, which includes 3 axial levels in this example.

Logically, a CRUD layer grows on the surface of the fuel rod, so we can say that a Surface has a CrudLayer. Therefore, a new class, called the CrudLayer class, is created to house all CRUD-related data and procedures. Each Surface object has a single CrudLayer object. As is the case for the Surface class, the CrudLayer class data is organized mostly into 1-D arrays that take an axial-level index and return the data at that rod level. Again, the axial meshing of the CrudLayer is conformal with the Surface and FuelRod classes.

The CrudLayer currently has only three procedures. The "CrudLayer::Initialize" procedure is called from the "Surface::Initialize" procedure to allocate all data arrays. The "CrudLayer::Grow_crud" procedure is called from "CTF_Coupling_Interface" to grow the CRUD between the previous T/H state point and the current one. Based on user input, this procedure will call either the surrogate or MAMBA1D. The "Grow_crud" procedure takes all simulation properties needed by MAMBA1D and the surrogate via its argument list. The "CrudLayer::Init_crud" procedure is used to save the current T/H state. This last procedure is needed because of the way the T/H-CRUD coupling algorithm works, which is further discussed in Section 4.

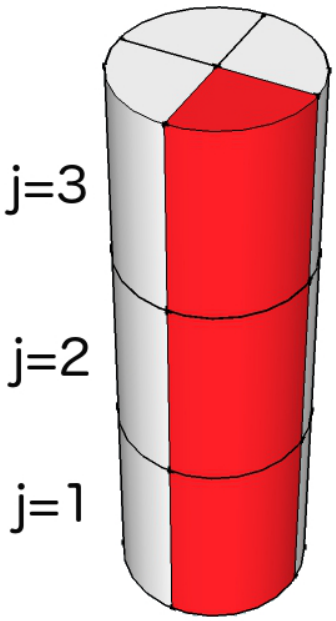

Figure 3. CTF model of a fuel rod having four surfaces and three axial levels.

3.2 CTF/MAMBA1D Coupling

CTF has been coupled with the subgrid version of MAMBA1D. The subgrid version can be called for an arbitrary number of rod surface segments. Building on the definitions of the previous section, a rod surface segment is one axial level of one surface. For example, the "j=1" level of the red surface in Figure 3 is a rod surface segment. If we so desired, we could call MAMBA1D for the entire CTF model in one shot (i.e., all rods, surfaces, and levels); however, doing so is not intuitive, and our definition of the CrudLayer essentially prohibits calling MAMBA1D in this way.

A single instance of MAMBA1D is called by the Grow_crud procedure of the CrudLayer class. This single call to MAMBA1D calculates new CRUD growth for all axial levels of the rod surface. If CTF were used to model a single rod, as shown in Figure 3, four calls to MAMBA1D would be made at the end of each state point. Each MAMBA1D call would solve three levels of the surface for which it was called.

3.3 Redesign of Multistate Input

MAMBA1D requires additional information that was not required of the surrogate. MAMBA1D takes two types of information: (1) global data that applies to all rod surface segments being treated in the call (for CTF, this means all axial levels of the rod surface) and (2) local data that is specific to each rod surface segment being treated in the call. The global data required by MAMBA1D is shown in Table 1; and the local, per-rod-surface-segment data is shown in Table 2. Each table gives the name of the parameter and a note on the value of the data or where the data is obtained.

Although much of this information can be extracted from the CTF input deck or the CTF solution, new information is needed pertaining to the coolant chemistry (e.g., dissolved boron, hydrogen, nickel), which can only come from the multistate driver input. Because of the large increase in the information needed from the multistate driver input file, the previous simple, rigid design was abandoned in favor of a more flexible means of obtaining information at each state point. This form is best demonstrated by example, which is shown in Figure 4.

Instead of taking the state data in columns all on one line, data is specifically entered in "state" group cards, similar to what is done in VERAIn. Also, a "control" card is entered to specify whether or not CRUD is modeled and whether the surrogate or MAMBA1D should be used. A group is specified by putting one of the identifiers, either "state" or "control," in square brackets. Any number of "state" groups could be entered, and all groups and parameters in the groups are optional. A multistate input file with no information can be provided, and the multistate driver will still run using all default values. Table 3 shows the information taken by the multistate driver and default values that will be used if the information is not provided.

Table 1. Input needed by MAMBA1D (single data per call)

Parameter name	Value
Num surfaces	Number of Surface axial levels
MAMBA1D timestep size (hr)	4 (MAMBA1D default)
CRUD growth start time (s)	Time at previous state
CRUD growth finish time (s)	Time at this state
Boron concentration (ppm)	Multistate driver input
Particulate nickel (ppb)	Multistate driver input
Core inlet temperature (K)	Core average from inlet BC

Table 2. Input needed by MAMBA1D (data per rod surface segment)

Parameter name	Value
Segment heat flux (W/m^2)	CTF solution
Segment surface temperature (K)	CTF solution
Turbulent kinetic energy facing segment (J/kg)	CTF solution

```
[control]
model_crud 1
crud_tool 1

[states]
[state]
day 0.0
inlet_temp 292.0
boron 1000.0
lithium 3.0
fesol 0.915
nisol 0.25
nipar 2.2
hydrogen 32.0E-6

[state]
day 90.0
boron 1000.0
lithium 3.0
fesol 0.915
nisol 0.25
nipar 2.2
hydrogen 32.0E-6
```

Figure 4. Redesigned multistate input file example.

Table 3. Multistate input file parameter list

Parameter	Description	Units	Default value
	[control] Group		
model_crud	Model CRUD (1) or do not model CRUD (0)	—	0
crud_tool	MAMBA1D (1) or surrogate (0)	—	0
run_state	Runs a specific, single state if set	—	Not set
	[state] Group		
day	Time in operation cycle	days	0.0
inlet_flow	Total mass flow rate into core	kg/s	CTF input deck
inlet_temp	Inlet temperature	C	CTF input deck
outlet_pressure	Pressure at core outlet	bar	CTF input deck
hydrogen	Dissolved hydrogen content in coolant	m^3/kg	3.2E-5
boron	Dissolved boron content in coolant	ppm	0.0
lithium	Dissolved lithium content in coolant	ppm	0.0
nisol	Soluble nickel in coolant	ppb	0.0
nipar	Particulate nickel in coolant	ppb	0.0
fesol	Soluble iron in coolant	ppb	0.0

Note that omitting any parameter will cause that parameter to be set to its default value for the "control" group or the first instance of the "state" group. For subsequent instances, the "state" group absent parameters will be left at their previous values, which either will be default or will have been set in a previously read "state" group.

4 Redefine CTF/CRUD Coupling Algorithm

The coupling algorithm originally involved doing a CTF solve for the first state and skipping the CRUD solve. On the second state, the CTF solve was done to produce a T/H solution; this was fed into the surrogate, and the surrogate was used to grow crud from State 1 to 2 using that T/H solution. After this, the multistate driver moved forward to the next state without carrying out any iteration between the two codes. This was a suitable first approximation, but it was not entirely correct.

Instead, the CRUD tool should take the average T/H solution that exists between two state points. Furthermore, there needs to be another CTF solve after the CRUD solve to update the internal fuel rod temperatures, which will be affected by the new CRUD deposits that impart increased thermal resistance in the fuel rod conduction equation. Furthermore, MAMBA1D will predict a steaming rate in the CRUD layer, which can lead to additional rod-to-fluid heat transfer and phase mass and energy transfer. However, as will be discussed in Section 7, it is assumed that all vapor generated in MAMBA1D solution space condenses back into liquid before entering the CTF solution space, resulting in no implicit heat transfer between the modeling regions.

Only one CTF solve is required to update the fuel temperature and complete the solution for the current state. Because this is a steady state simulation (all heat generated in the fuel rod leaves the fuel rod surface), there is no need for further iteration after the CTF update because the thermal resistance does not affect the MAMBA1D inputs (i.e., rod surface temperature, heat flux, coolant properties, and erosion forces). The new coupling algorithm is summarized in the flowchart of Figure 5.

As the figure shows, the multistate input file is read, CTF is initialized, and the driver enters the state loop, as before. The power distribution is set via the HDF5 file, if one is made available. Next, other boundary conditions (inlet temperature, flow, and outlet pressure) are set, and the first T/H solve is performed. After the first T/H solve, the CRUD solve is not actually a solve; rather, the CrudLayer::Init_crud procedure is called to simply save the current T/H solution facing each rod surface. After the T/H solution is saved, the multistate driver skips ahead to the next state.

In the second and subsequent states, power distribution and boundary conditions are set and the T/H solve is done. However, the CRUD solve in these states actually involves growing CRUD. The call to CrudLayer::Grow_crud is made, which will average the current T/H solution with the previous state T/H solution in a linear fashion. This averaged T/H solution is input to the CRUD tool to grow the CRUD over the time that has lapsed between the two states. After new CRUD deposits are made, CTF is called once more to update the internal rod temperature distribution. At the completion of each state, edits are written to the HDF5 file.

Note that the new multistate input, "run_state" (see Table 3), allows the user to specify a single state to run. This is useful if we wish to run a specific state from an HDF5 file that is produced by VERA-CS. If this option is selected, the multistate driver will simply set the power distribution for that state and for the boundary conditions specified in the multistate input file, run CTF, and then exit.

The specific coupling between CTF and MAMBA1D is illustrated with Figure 6. This figure demonstrates that CTF is solved at the states, whereas the CRUD tool is solved from state to state. CTF is treated as a steady-state code, whereas the CRUD tool is treated as transient. At the end of states 2 and above, an additional CTF solve is done to update internal rod temperatures.

As a result of this coupling work, a few new datasets will be written to the HDF5 file when a coupled T/H-CRUD simulation is performed. These include

- pin_avg_crud_thickness (volume-average CRUD thickness around the azimuth of the pin for each channel level (units of microns))

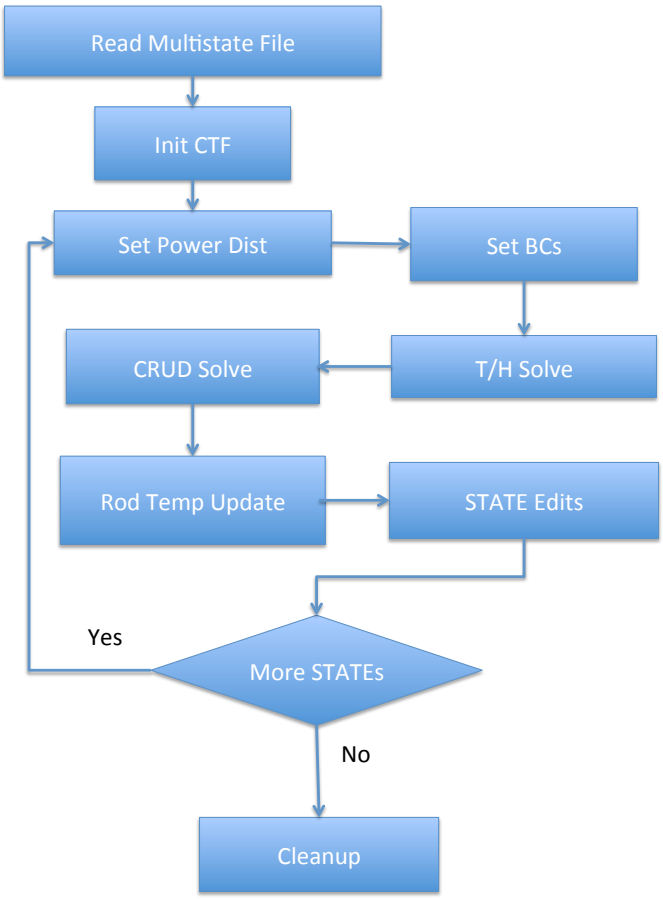

Figure 5. Solution algorithm for the multistate driver.

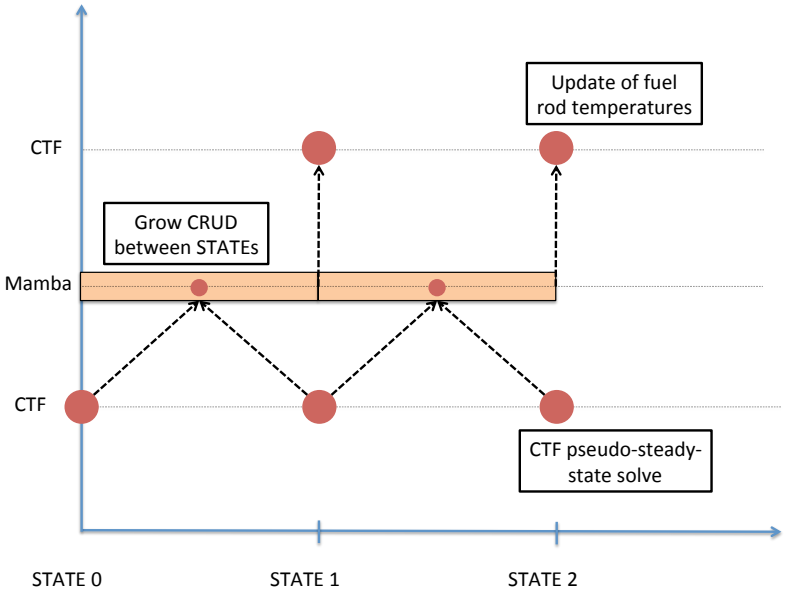

Figure 6. Illustration of the CTF/MAMBA1D coupling algorithm.

- pin_avg_crud_borondensity (area-weighted average CRUD boron density around the azimuth of the pin for each channel level (units of kg/m^2))
- pin_avg_crud_massdensity (area-weighted average CRUD mass density around the azimuth of the pin for each channel level (units of kg/m^2))
- pin_max_crud_thickness (single value that gives maximum CRUD thickness and its location in the core (units of microns)

5 Incorporating MAMBA1D

The CrudLayer::Grow_crud procedure will make the call to the MAMBA1D interface, but only if the MAMBA1D source is made available during the CTF build process. The actual call to MAMBA1D will be "ifdef"ed out of the code otherwise, and the user will receive an error message stating that the simulation cannot be done. The MAMBA1D code contains 3 files: (1) the core MAMBA1D package, "mamba1d.f", (2) a header file for the package, "mamba1d.h", and (3) an interface to MAMBA1D, "mamba_cfd.f". Additional files include programs in "mamba1d_testdriver.f" and "mamba1d_testdriver_noboil.f," which act as regression tests for the software.

These files have been set up in a Git repository called "MAMBA" that is now hosted on casl-dev. The files have been made into a TriBITS package, also named "MAMBA," with the two regression test files made into two automated regression tests. The COBRA-TF TriBITS package is modified to include MAMBA1D as an optional package dependency. If found, the build will include MAMBA1D in the build and the user will be able to perform coupled CTF/MAMBA1D simulations.

To protect the coupling feature, three regression tests are added to the COBRA-TF package: (1) a single rod modeled over 360 days in 30 day increments (13 states), (2) a quarter symmetry model of a 5 assembly cross of simple 3×3 rod bundles modeled over 360 days in 90 day increments (5 states), and (3) a quarter symmetry cross the same as in item 2 but modeled in parallel. These tests use the "multistate_diff" utility, which checks the following output over all states of the simulation:

1. coolant temperature
2. coolant density
3. volume-average clad temperature
4. volume-average fuel temperature
5. rod powers
6. CRUD thickness
7. max coolant temperature
8. max clad temperature
9. max fuel temperature
10. inlet density
11. exit density
12. exit temperature
13. inlet temperature

Items 1–6 are calculated for each relevant computational cell in the model; they are checked against gold file values for each cell. The remaining items in the list are calculated only once in the model, but they are also checked against their gold-file counterparts. This set of information is checked for every state in the simulation to within a relative tolerance of 0.1 % and an absolute tolerance of 1.0E-6. If the value changes by less than either of these tolerances, the regression test passes.

6 CRUD Erosion Model

MAMBA1D takes TKE as input to model the CRUD erosion experienced over a period of time. The challenge in this coupling is that CTF does not explicitly model this physical flow property as a CFD code with an advanced turbulence model does, so it is necessary to estimate the term from another solved quantity in CTF. It is known that there is a relationship between shear stress, a term that CTF does calculate, and TKE [6], so an approach to convert shear to TKE was developed.

Two approaches are taken in solving this issue: (1) a physics-based model found in the literature for converting from shear to TKE and (2) a method for calculating a tuning coefficient that delivers a specified model-wide average TKE to MAMBA1D. These two approaches are further discussed in the following subsections. The second approach is the default approach for calculating TKE and modeling CRUD erosion in MAMBA1D.

6.1 Physics-Based Model

Work has been done by Bradshaw [6] and Harsha [7] to correlate TKE to turbulent shear stress in turbulent boundary layers and wakes using experimental data. Bradshaw made measurements of velocity profiles in turbulent boundary layers in the National Physical Laboratory [8] in Great Britain in the 1960s using hot-wire anemometry. Measurements were made for three different sets of conditions: zero pressure gradient, mild adverse pressure gradient, and strong adverse pressure gradient. In CTF, we mostly encounter boundary layers in favorable pressure gradients, so we assume that Bradshaw's findings are extensible to equilibrium boundary layers in all types of pressure gradients. A plot of the boundary layer velocity profile for the three types of boundary layers measured by Bradshaw is shown in Figure 7.

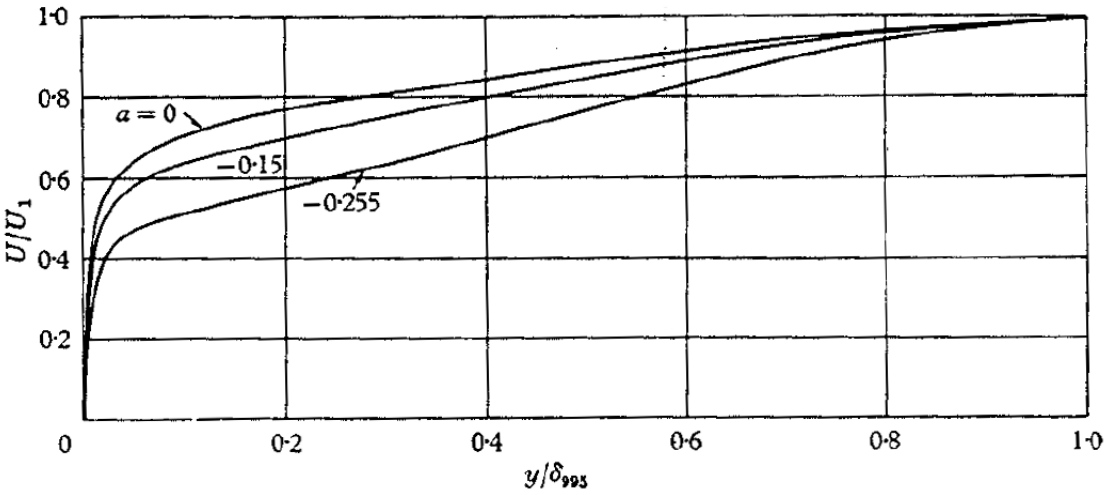

Figure 7. Mean velocity profiles of boundary layers studied by Bradshaw at 83 in. **from flow tunnel inlet.**

Bradshaw plotted the ratio of the local shear stress to TKE for each of these profiles as shown in Figure 8. The q^2 term in the y-axis label is defined as $\overline{q^2} = \overline{u'^2} + \overline{v'^2} + \overline{w'^2}$. Since the TKE is defined as $K = 1/2(\overline{u'^2} + \overline{v'^2} + \overline{w'^2})$, we can relate the two quantities as $K = 1/2\overline{q^2}$.

Using a digitizer, the data for the zero pressure gradient line (a=0) is converted to tabular format and the ratio is converted to $\tau/\rho K$ by multiplying all data points by a factor of two. This gives a local relationship between shear stress and TKE throughout the boundary layer. The shear stress is a term that can be calculated in CTF from the two-phase pressure drop. This can be extracted as follows:

$$\tau_w = \frac{\Delta P_{\text{fric}}}{\Delta X} \frac{A_{\text{chan}}}{P_{w,\text{surf}}} \tag{1}$$

The frictional pressure drop, $\frac{\Delta P_{\text{fric}}}{\Delta X}$, is calculated for each scalar mesh cell using the model of Wallis [9]. By multiplying this by the cross-sectional area of the cell, A_{chan}, we obtain the force per unit of length acting on the surfaces adjacent to the flow channel. Dividing this value by the wetted perimeter, $P_{w,\text{surf}}$, of the adjacent surface provides the shear force acting on the surface. This shear force can be used with the relationship discovered by Bradshaw to obtain an estimate of TKE in the boundary layer on the rod surface. Note, however, that the shear stress in CTF is an integral value (i.e., the average shear stress acting on that surface over the entire boundary layer thickness). Therefore, we first look to reduce Bradshaw's relationship to an average value that applies throughout the entire thickness of the boundary layer.

The digitized ratio between τ_w and K is shown in Figure 9 along with a curve fit to the data. The curve used to fit the data is of the form, $\frac{\tau_w}{\rho K} = -(\frac{y}{\partial} + a)^4 + b$. A reasonable fit is achieved with coefficients a and b set to -0.53 and 0.31, respectively. Taking the integral of this correlation from 0.0 (the wall) to 1.0 (the top of the boundary layer), provides a value of 0.297, leading to the following relationship:

$$\tau_w = 0.297\rho K \tag{2}$$

This compares favorably with the relationship between shear and turbulent kinetic energy that Harsha [7] presented for turbulent wakes, which was $\tau_w = 0.3\rho K$.

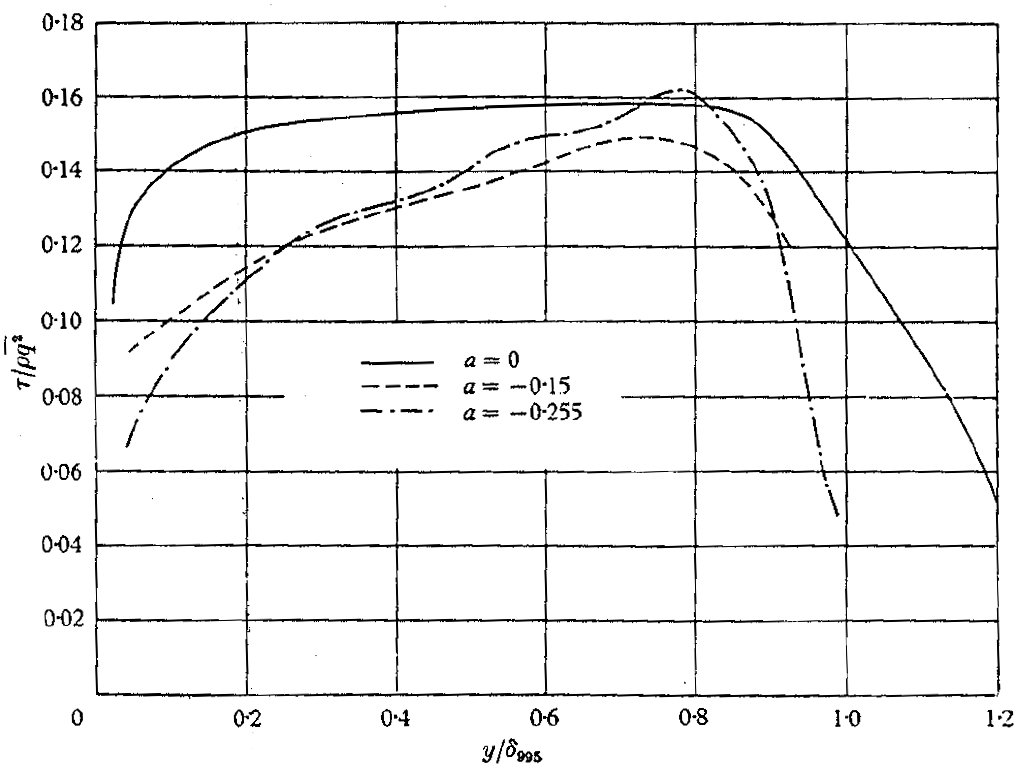

Figure 8. Ratio of local shear stress to turbulent kinetic energy throughout the boundary layer thickness.

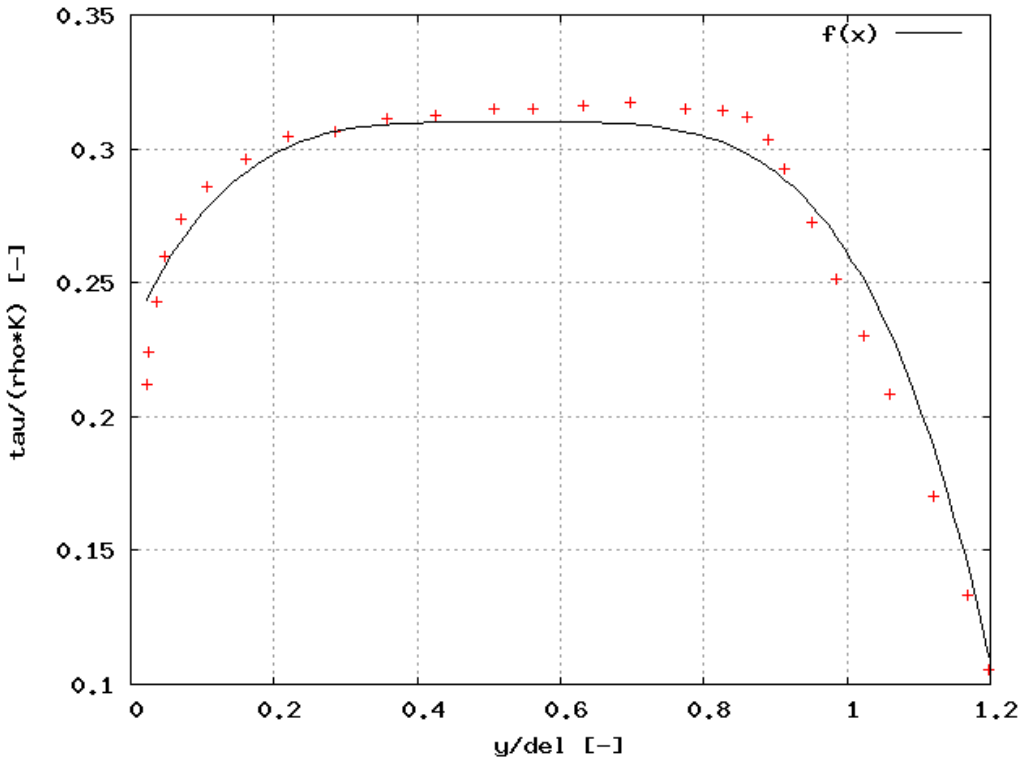

Figure 9. Ratio between local shear and turbulent kinetic energy for a boundary layer in a zero pressure gradient.

To test this relationship, a CTF model is run for Watts Bar, which is a Westinghouse 4-loop pressurized water reactor (PWR). This model is described in greater detail in Section 8. The rod surface shear stress, which is back-calculated from the CTF-calculated two-phase pressure drop, is extracted for each rod surface in the model. The shear stresses experienced on each rod surface are presented in Figure 10, where the x-axis is the rod level in CTF and the y axis is the shear acting on the surface of the rod. The average shear stress (not area-averaged) in the core is 32.33 $\frac{\mathrm{N}}{\mathrm{m}^2}$.

To get a sense of the "correctness" of this value, a hand-calculation is done in Eq. (3) using prototypical PWR operating conditions and the Darcy-Weisbach equation to determine expected shear. For the calculation, a friction factor of 0.013 is obtained from the Moody chart for smooth surfaces with Reynolds number of 500,000. Considering an average velocity of 6 $\frac{\mathrm{m}}{\mathrm{s}}$ and an average density of 700 $\frac{\mathrm{kg}}{\mathrm{m}^3}$, the expected shear is about 41.0 $\frac{\mathrm{N}}{\mathrm{m}^2}$, which is in the ballpark of the number back-calculated from CTF.

$$\tau_w = \frac{f\rho V^2}{8} = \frac{0.013(700kg/m^3)(6m/s)^2}{8} = 41.0N/m^2 \tag{3}$$

The associated TKE values are calculated using the relationship presented in Eq. (2). The spread of values for the Watts Bar model is given in Figure 11. The average TKE in the core is 0.158.

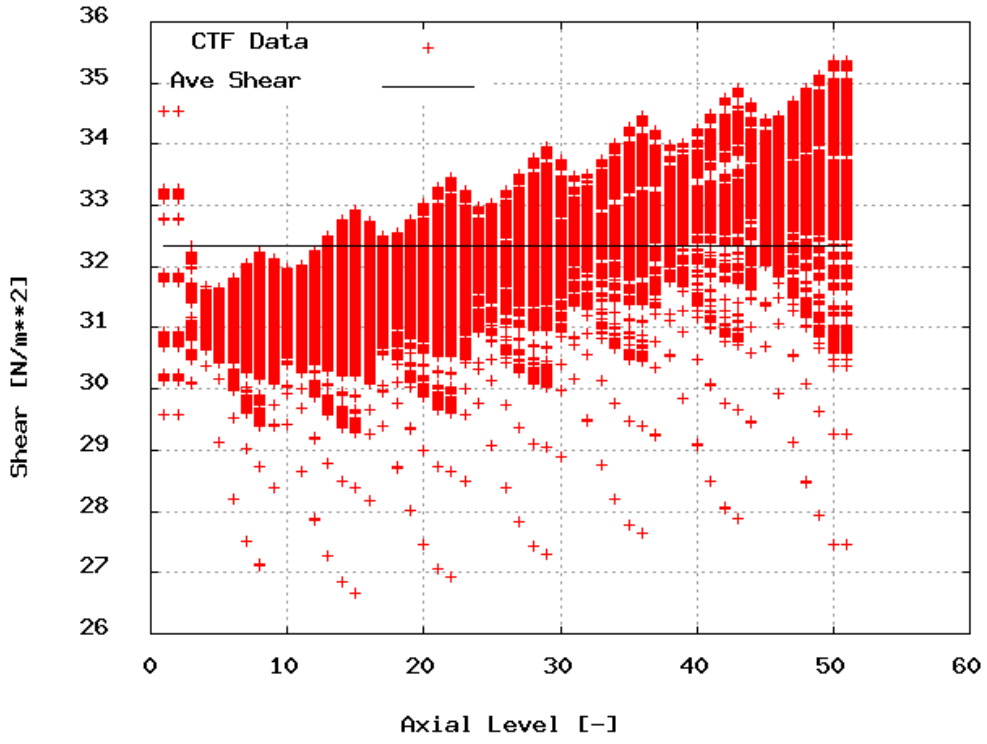

Figure 10. Rod surface shear stresses experienced in the CTF model of Watts Bar.

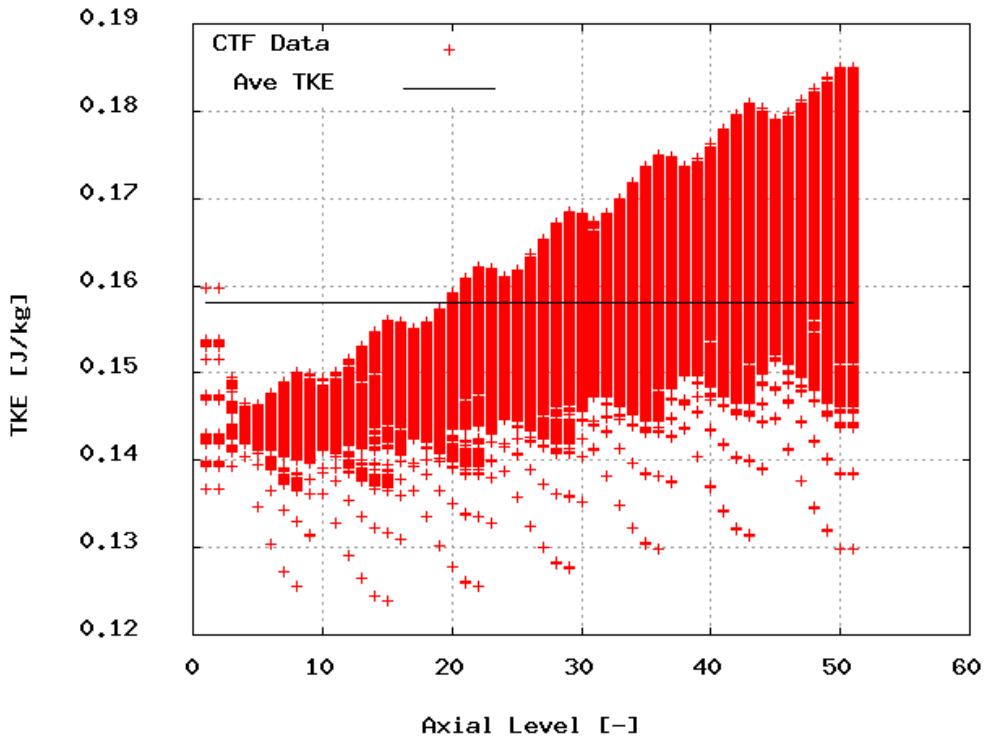

Figure 11. Rod surface turbulent kinetic energy calculated using model of Bradshaw and CTF-back-calculated rod wall shear.

6.2 Tuning Coefficient Approach

While researching shear/TKE models in the literature, it was discovered that MAMBA1D is actually tuned to achieve a specific erosion rate (likely measured from the Walt loop [10]) for a specific TKE value. A "standard" TKE of 0.1 $\frac{\text{J}}{\text{kg}}$ was considered in developing this model. Therefore, passing MAMBA1D a TKE of 0.1 $\frac{\text{J}}{\text{kg}}$ will result in an expected amount of CRUD erosion for typical PWR operating conditions. As demonstrated in the result of Figure 11, the average TKE predicted by CTF for Watts Bar using the Bradshaw model is 0.158. Since shear and TKE are linearly related, this means that erosion rates predicted using the Bradshaw model would be 58 % higher than the expected values.

To mitigate this problem, a second approach for converting shear to TKE is implemented. This works by calculating a surface-area-weighted shear for the entire model and then using that to develop a shear/TKE conversion coefficient as shown in Eq. (4).

$$c = \frac{0.1}{\overline{\tau}} \tag{4}$$

The units of this conversion factor are J-ft^2/kg-lbf. This coefficient is multiplied by the local shear stress on each rod surface segment to obtain a local TKE in the units needed by MAMBA1D. Using this normalization, the core-average TKE passed to MAMBA1D will be the expected value of 0.1 $\frac{\text{J}}{\text{kg}}$. This approach is the default method for calculating TKE to be handed to MAMBA1D in the CTF/MAMBA1D coupling.

Although a physical model is ideal, the tuned model is currently the default, since MAMBA1D has been tuned to use this value. In the future, the MAMBA1D erosion model should be studied in more detail to determine if this tuned coefficient can be eliminated in favor of a more physical approach.

7 Boiling Model

This section discusses how boiling is treated in CTF and MAMBA1D, as each code has its own separate model. The MAMBA1D model is designed to treat boiling in the crud layer and its effect on crud deposition and heat removal from the crud. The CTF model is designed to model vapor generation and heat transfer on the surfaces of clean rods. Consideration is given here to how these two models should be combined. Section 7.1 starts by reviewing the model in MAMBA1D.

7.1 MAMBA Boiling Model

The MAMBA1D boiling model is used to calculate the volumetric heat removal rate in the CRUD layer due to chimney boiling, as shown in Eq. (5).

$$q_j''' = \frac{h_{b,j}(T_{\text{CRUD,j}} - T_{\text{sat}})}{\Delta r_j} \tag{5}$$

Since MAMBA solves conduction only in the 1-D, radial direction, there is no temperature variation in the azimuthal or axial directions of the CRUD layer. Therefore, the heat transfer rate will vary only in the radial direction as a result of variation in the CRUD temperature, $T_{\text{CRUD,j}}$. The index, j, has been used to denote the radial layer of the CRUD. The liquid saturation temperature, T_{sat} is a fixed constant of 345.548 °C in MAMBA. The denominator, Δr_j, is the chimney length. The expression is divided by the thickness of the CRUD layer at level j to convert the heat flux into a volumetric heat rate. Finally, the $h_{b,j}$ term is the heat transfer coefficient between the CRUD and water in the chimney. This value is calculated as follows:

$$h_{b,j} = H_c f A_{c,j} N_c \tag{6}$$

The term, H_c, is a fixed chimney heat transfer coefficient, which is a constant value of 0.067 W/cm^2 K. The f term is a scaling factor, which is a constant of 3.1818140581634617. N_c is the chimney number density (the number of chimneys per square centimeter of rod surface); it is a fixed value of $4.8{\cdot}10^4$ chimneys/cm^2. Finally, A_c is the surface area of the chimney; it is calculated assuming that the chimney is cylindrical in shape. This is shown in Eq. (7).

$$A_{c,j} = 2\pi r_c \Delta r_j \tag{7}$$

The radius of the chimney is r_c and, as before, Δr_j is the chimney length at level j. The chimney radius is taken to be a constant of 4 microns.

MAMBA1D does two things with the chimney boiling heat flux: (1) uses it in the conduction equation solution to calculate the CRUD heat removal rate and (2) uses it to calculate the vapor generation rate in the chimneys. The CRUD heat removal rate is not directly returned to CTF. Rather, MAMBA1D uses the heat removal rate to calculate the CRUD temperature distribution. The CRUD temperature distribution is then used to calculate a total CRUD thermal resistance, which is returned to CTF. CTF then directly uses this term in its rod conduction equation to represent the CRUD temperature drop that MAMBA1D has calculated. The vapor generation rate is returned to CTF. It is calculated from the boiling heat flux in MAMBA1D as in Eq. (8).

$$\dot{m}_j = \frac{q'''_{b,j} \Delta r_j}{h_{fg}} \tag{8}$$

The latent heat of vaporization, h_{fg}, is a constant of 951 $\frac{\text{J}}{\text{g}}$. The mass generation rate is summed for all radial mesh cells and the total is returned to CTF.

As seen in this section, there are constants used in the MAMBA1D boiling model for liquid saturation temperature and latent heat of vaporization. In the future, it will be possible to remove these constants by taking them via the MAMBA1D coupling interface. This would ensure consistency with the steam table properties being used by the T/H code, which are used to convert the CTF boiling heat flux to mass transfer and vice versa.

7.2 Combination of the Models

The solution space of the two codes is shown in Figure 12. The CTF solution space includes everything inside the fuel rod (fuel, gap, clad) and the fluid region. Each fuel rod region has an associated thermal resistance that is used in the CTF conduction equation solution. Actually, the crud region also has a thermal resistance that is used in the CTF conduction equation solution; however, the thermal resistance is solved by MAMBA1D and given to CTF as a source term. The fluid also includes a thermal resistance that captures heat transfer between the rod and fluid. This will consist of forced convective heat transfer and surface boiling in the CTF solution.

The concern in this system is whether the boiling that is happening inside of the crud (calculated by MAMBA1D) should impact the CTF solution. Specifically, the concern is whether the effect should act to transfer heat from within the crud layer out into the fluid in CTF. An assumption was made that all vapor generated in the crud layer condenses as it moves to the top of the crud layer so that no vapor moves into CTF solution space. In this way, all heat removed from lower in the crud layer would be redeposited into upper regions of the crud layer.

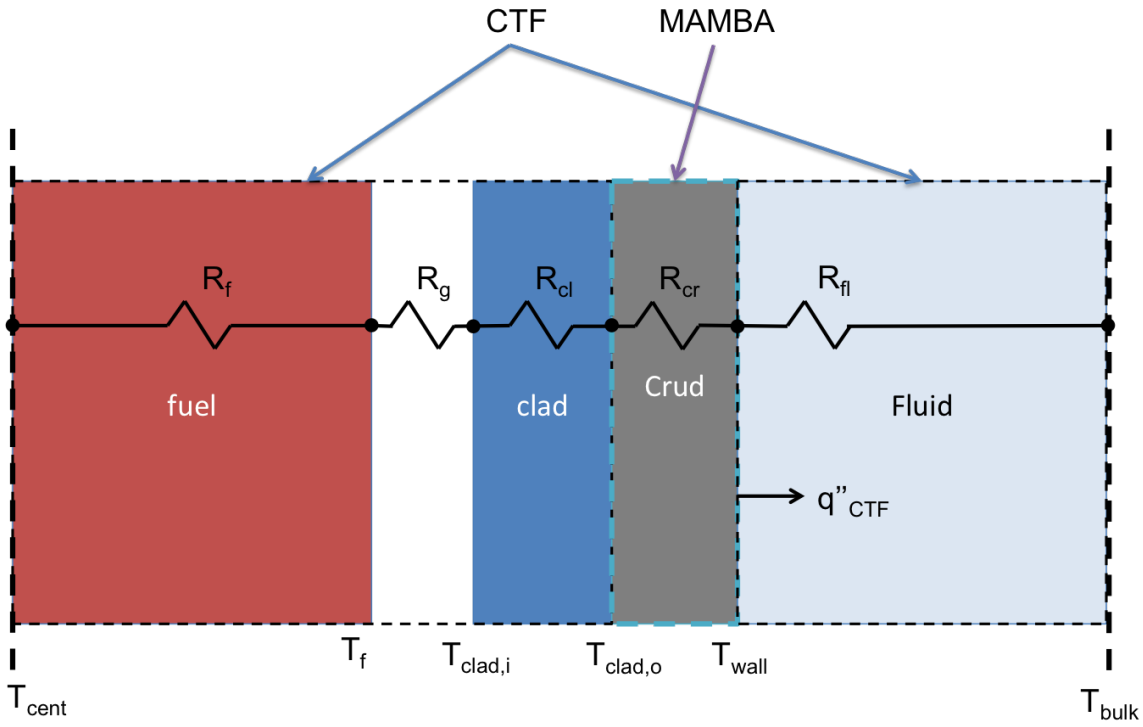

Figure 12. Visualization of CTF and MAMBA1D solution spaces starting from fuel centerline (left) and moving to channel centerline (right).

In all likelihood, MAMBA1D has been tuned to capture all boiling effects, since both surface and internal boiling will result in crud deposition. In this case, there may be a double counting of the surface boiling effect in the two codes. Since we assumed that all vapor condenses in the MAMBA1D solution space, there is no concern with regard to adding the crud boiling as a heat transfer mechanism in CTF. The following section shows a comparison of crud boiling effects (predicted by MAMBA1D) and surface boiling effects (predicted by CTF), which shows that including the MAMBA1D crud boiling as a CTF heat transfer effect would lead to a significant reduction in rod surface temperature. However, there remains the issue of whether the CTF surface boiling should be disabled in regions of crud growth. This would affect the rod surface temperature, which is a boundary condition to MAMBA1D. Disabling surface boiling would lead to a higher surface temperature and thus more crud deposition and possibly more boron precipitation. This issue should be investigated further in the future.

7.3 CRUD Boiling Impact

A single rod case was run at PWR operating conditions of 155.132 bar psi, 3500 $\frac{\text{kg}}{\text{m}^2\,\text{s}}$, and 17.7 MWt to investigate the impact of the CRUD boiling term. The case was run over a long period of time to grow thick CRUD deposits. CRUD thickness increased from 0 to about 60 microns by the end of the simulation. During the simulation, a single rod surface located in an area of the model that experienced thick deposits was observed. Considering that CRUD dynamics will be almost entirely dependent on local quantities, it is suitable to observe local T/H data for that single surface, which is shown in Table 4.

Table 4. Local surface operating conditions for boiling sensitivity study

Parameter	Value
Pressure	155.552 bar
h_{fg}	966.07 $\frac{\text{J}}{\text{g}}$
T_{sat}	345.19 °C
A	5.46 cm^2

For the sake of comparison, the local saturation temperature in CTF is 345.19 °C, which compares favorably with the MAMBA1D constant value of 345.548 °C. However, there is a more significant difference between the local h_{fg} term— 966.07 $\frac{\text{J}}{\text{g}}$ in CTF compared with 951.0 $\frac{\text{J}}{\text{g}}$ in MAMBA1D. Table 5 shows the evolution of CRUD thickness, CRUD chimney boiling predicted by MAMBA1D, and surface boiling predicted by CTF using the Thom model. Results show that the CRUD boiling rate, $\dot{m}_c$ increases with CRUD thickness; but generally it is about 4 orders of magnitude larger than the CTF surface boiling rate, $\dot{m}_{\text{surf}}$.

Table 5. Comparison of CRUD chimney boiling (predicted by MAMBA1D) and rod surface boiling (predicted by CTF)

State	CRUD thickness [micron]	$\dot{m}_c$ [kg/s]	$\dot{m}_{surf}$ [kg/s]
1	0.0	0.00E+0	8.00E-7
2	2.3	1.47E-3	8.00E-7
3	4.5	1.49E-3	8.00E-7
4	6.8	1.51E-3	8.00E-7
5	9.1	1.52E-3	8.00E-7
6	11.4	1.54E-3	8.00E-7
7	13.8	1.55E-3	8.00E-7
8	16.1	1.57E-3	8.00E-7
9	18.5	1.59E-3	8.00E-7
10	20.9	1.60E-3	8.00E-7
11	23.3	1.62E-3	8.00E-7
12	25.8	1.64E-3	8.00E-7
13	28.2	1.65E-3	8.00E-7
14	35.8	1.70E-3	8.00E-7
15	43.5	1.75E-3	8.00E-7
16	51.4	1.81E-3	8.00E-7
17	59.3	1.65E-3	8.00E-7

8 Feature Testing

8.1 Watts Bar Demonstration

To demonstrate that the capability works and scales up to large problems, a quarter symmetry model of Watts Bar Unit 1 was run using the multistate driver with the MAMBA1D CRUD model activated. The case was run over an 18 month (540 day) cycle divided into 90 day periods, leading to 7 state points. A uniform set of operating conditions were used throughout the cycle simulation (see Table 6). The Watts Bar geometry is described in more detail in the report CASL-U-2012-0131-003 [11]. The power distribution for this case was obtained by running a coupled MPACT-CTF simulation at 100 % rated power and flow. The coupled neutronics-T/H simulation was run only for the sake of obtaining a realistic power distribution for this case. Note that whereas the inlet temperature in the MPACT/CTF simulation was 292.6 °C, the inlet temperature of the CTF/MAMBA1D simulation was increased to 298.0 °C to provoke additional boiling and CRUD growth.

Core heat flux is visualized in an isometric cutaway of the core, shown in Figure 13. This heat flux is applied for the entire cycle simulation. It leads to the steaming rate shown in Figure 14. The steaming is shown as an overlay on the translucent heat flux plot. It is apparent that maximum steaming occurs in the hottest assemblies, just above the mid-line of the core; that is to be expected, since this is where subcooling will be lowest. Note also that the steaming is affected by the grid spacer cooling enhancement. Steaming stops downstream of the grids where turbulence has been increased and the boundary layer is disrupted. This effect is better visualized if the model is rotated to a side view. This is shown in Figure 15.

The selected operating conditions lead to CRUD growth throughout the cycle. Figure 16 shows locations of CRUD deposits at the end of the cycle. Deposits reach a maximum thickness of about 21 µm. The deposits occur in the same locations as the steaming locations in the core. Furthermore, the grid cooling enhancement effects are visible in the side view shown in Figure 17.

Table 6. Operating conditions for full-core CTF/MAMBA1D simulation

Parameter	Value	Unit
Pressure	2,250	psi
Power	3,411	MW
Flow	131.68	Mlbm/h
Inlet temp	568.4	F
Boron	1000	ppm
Lithium	3.0	ppm
Fe_{sol}	2.0	ppb
Ni_{sol}	0.25	ppb
Ni_{par}	2.5	ppb
Hydrogen	32×10^{-6}	ppm

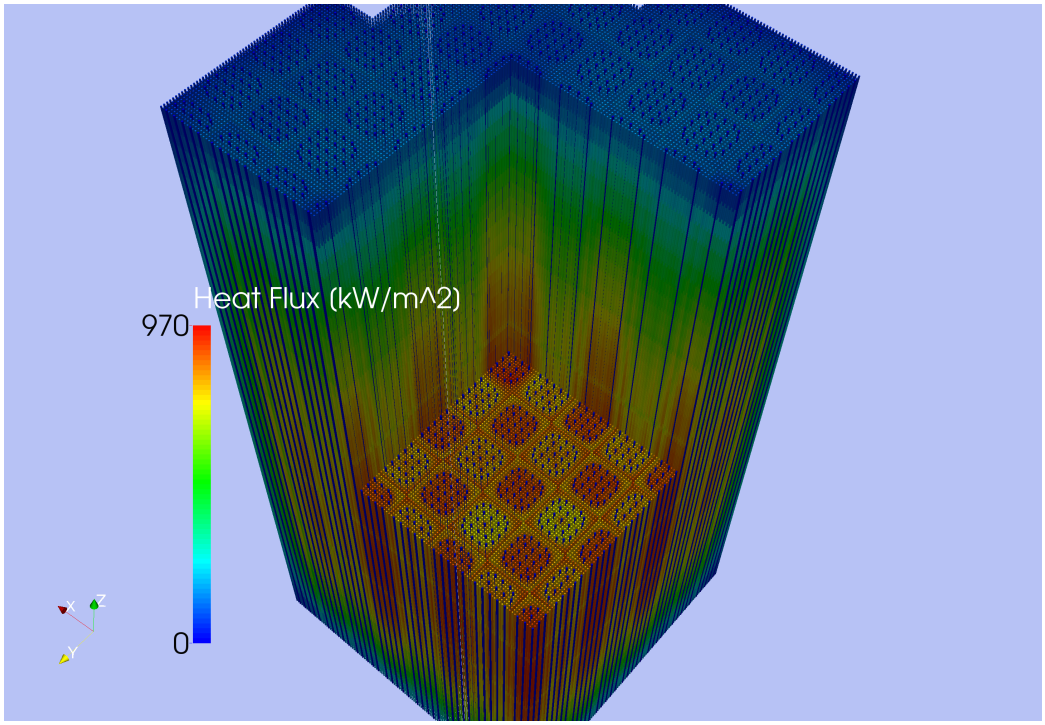

Figure 13. Watts Bar Unit 1 heat flux applied over cycle simulation.

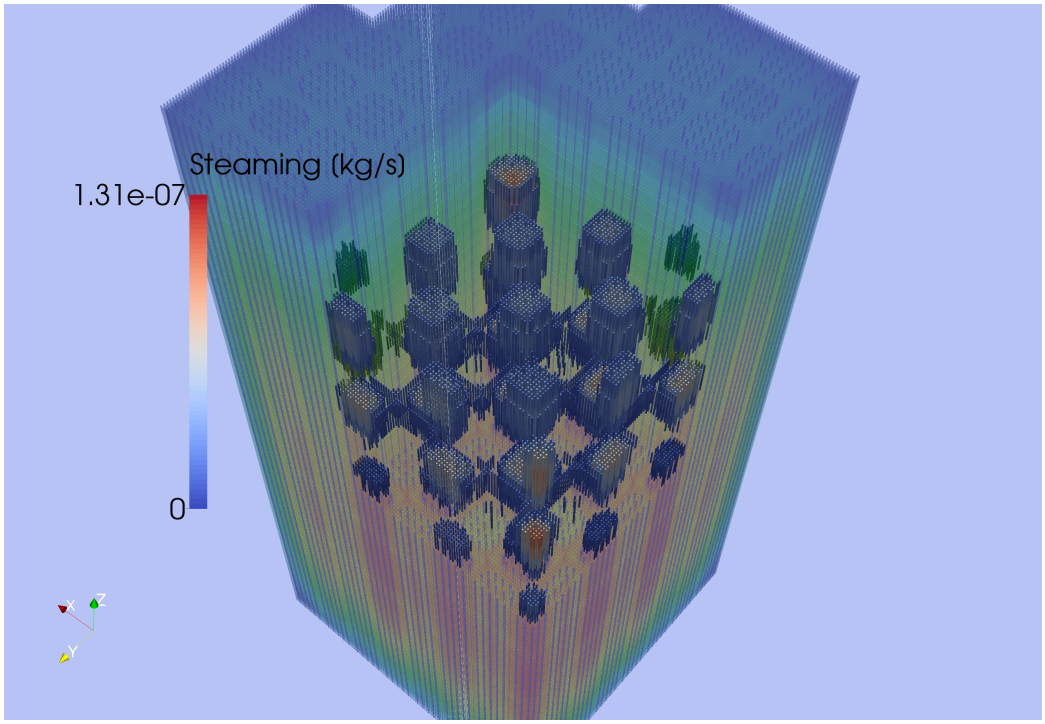

Figure 14. Watts Bar Unit 1 steaming rate.

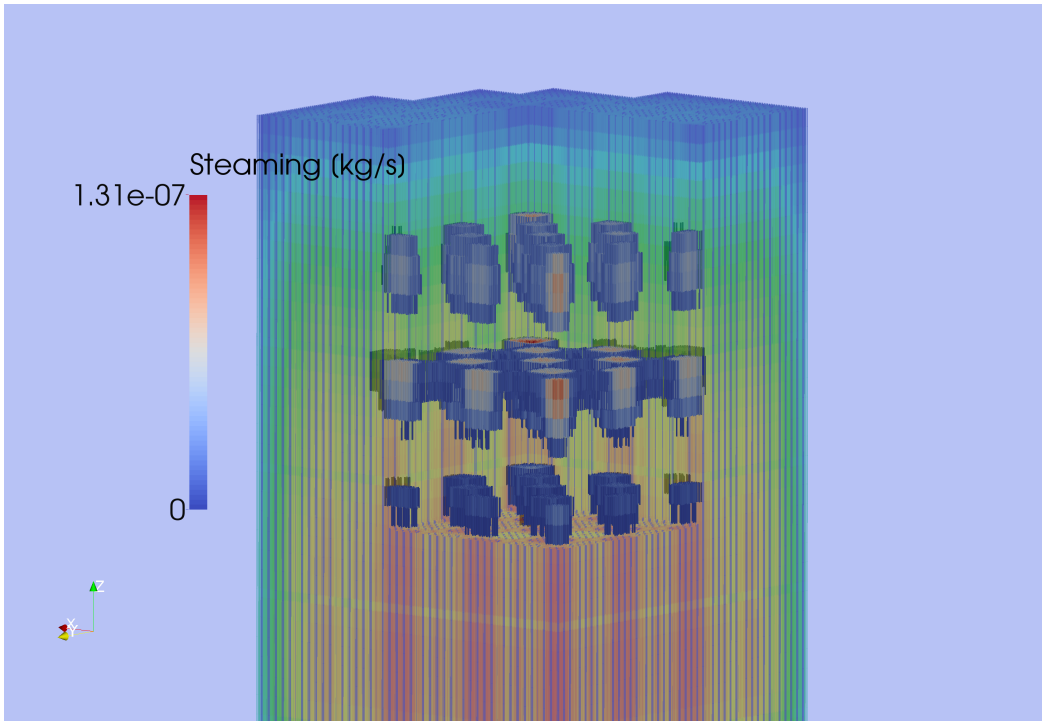

Figure 15. Watts Bar Unit 1 steaming rate (side view).

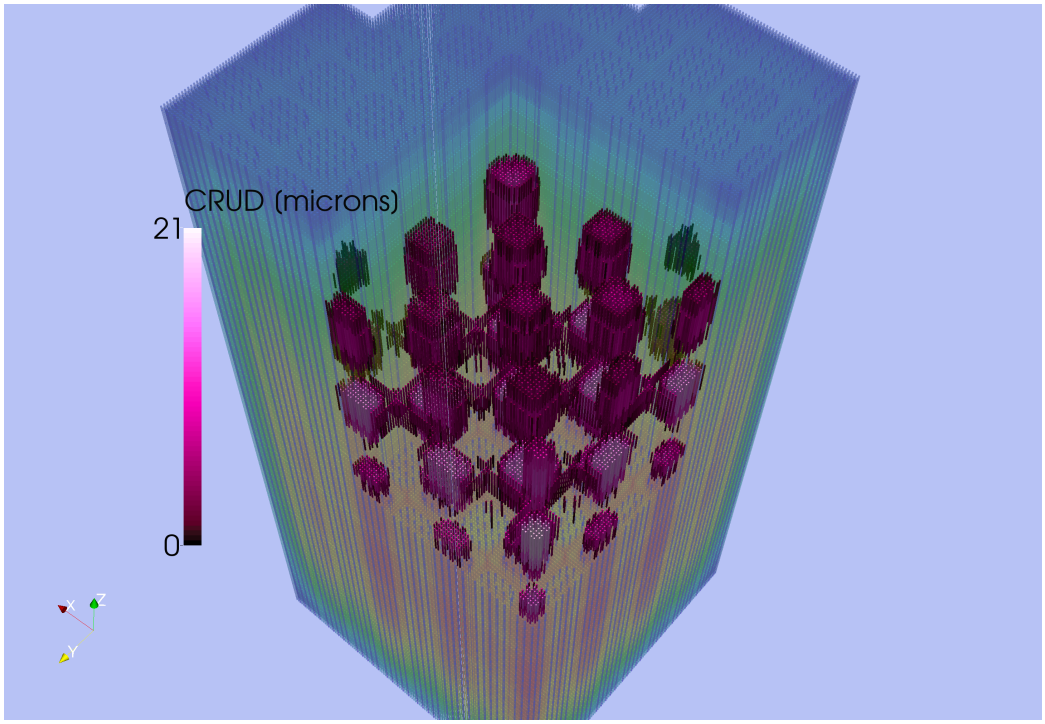

Figure 16. CRUD thickness at the end of the cycle simulation.

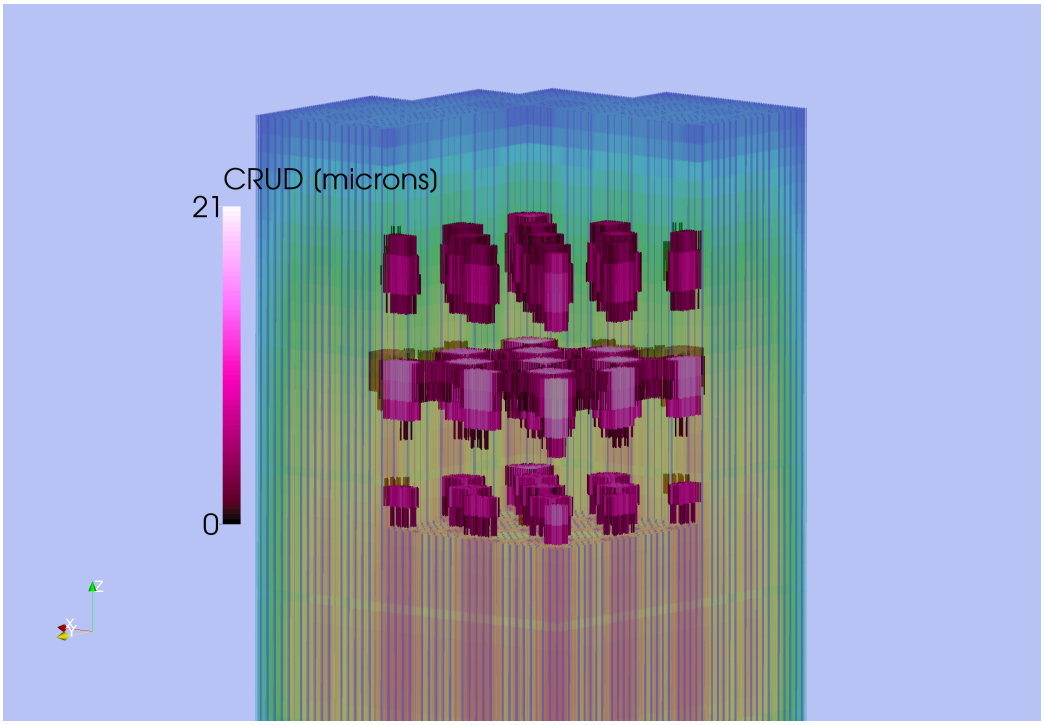

Figure 17. CRUD thickness at the end of the cycle simulation (side view).

8.2 Seabrook Validation

The Seabrook Unit 1 core is a 4-loop Westinghouse PWR. Cycle 5, which operated from December 1995 to May 1997, experienced both core-wide CIPS and CILC due to heavy CRUD deposits; the total cycle length was about 500 effective full power days.A total of five fuel rods failed in four different assemblies. The four failed fuel assemblies were fresh fuel at the beginning of the cycle and were of the Westinghouse 17×17 V5H design. Figure 18 shows the Cycle 5 layout with the four assemblies that experienced failure highlighted in red [12]. Assemblies G69 and G70 were modeled as part of this validation study.

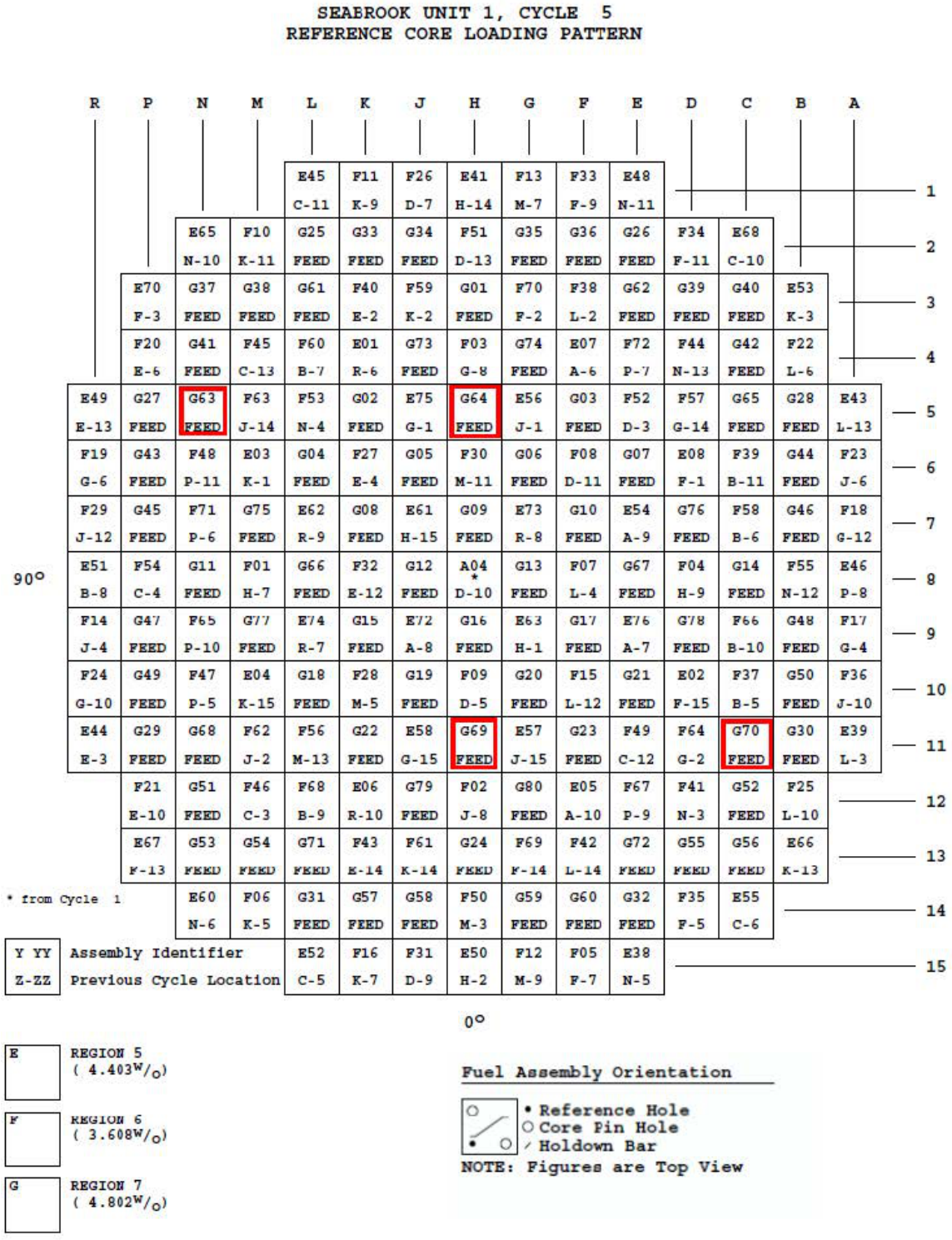

Figure 18. Diagram of the Seabrook cycle 5 core design with the assemblies experiencing failures highlighted in red

8.2.1 Model

The power distribution for this case was obtained from a nodal code simulation of the full-core Seabrook Cycle 5 using ANC. The operating conditions for the simulation are shown in Table 7.The axial mesh for the ANC simulation includes 24 axial nodes.

The ANC output file was converted to the standard VERA-CS HDF5 file format so that CTF could directly read this detailed power distribution. During the conversion process, the axial power distribution was refined so that there were 72 uniform axial mesh cells in the HDF5 file. The refinement was done so that a more refined axial mesh could be used in CTF, since 24 nodes is too coarse for a T/H solution.

The ANC simulation models the entire operating cycle, which is divided up into 13 state points. The burnup and plant chemistry data is shown in Table 8. The chemistry information is set in CTF and MAMBA1D via the multistate driver input file.

The CTF model is built from the CASL Problem 6 model, which is a standard 17×17 Westinghouse fuel assembly. The geometry for this case is shown in Table 9. The axial mesh is made to match the axial mesh in the VERA-CS HDF5 file, which leads to a uniform mesh with each mesh cell being 5.08 cm high. Since this mesh is not consistent with the one used in Problem 6, the grid placement must be modified slightly. This is considered suitable because (1) we do not have explicit specification of the grid locations; and (2) there are no grids in the ANC model, so the axial power distribution does not reflect their presence.

The placement of grids is shown in Figure 19. Because the axial mesh is uniform, the axial height of the grids had to be changed to 10.16 cm so that their top and bottom edges would land on mesh cell boundaries. Since CTF treats a spacer grid as a planar loss coefficient, this has no effect on the T/H solution except to shift the upstream edge of the grid (where the loss coefficient is applied) down further in the model. The CTF grid spacer cooling enhancement model is activated to capture heat transfer enhancement (and thus boiling and CRUD growth suppression) effects downstream of the spacer grids.

The operating conditions for the model are mostly set from Table 7. Since CTF does not take a volumetric mass flow rate as input, it is necessary to convert the mass flow rate to units of $\frac{\text{kg}}{\text{s}}$. The value also must be scaled down to the single assembly model. The first law (Eq. [9]) can be used to calculate mass flow rate, since we know core power and enthalpy rise.

$$\dot{q} = \dot{m}\Delta h \tag{9}$$

Table 7. Operating conditions for Seabrook Cycle 5

Parameter	Value	Units
Inlet flow	1,517,188.3	L/min
Bypass flow	5.8	%
Inlet temperature	292.7	C
Core power	3,411	MWt
Gamma heating	2.6	%
Outlet pressure	155.132	bar

Table 8. Seabrook Cycle 5 burnup, power, and chemistry

Day	Burnup [GWd/MTM]	Lithium [ppm]	Sol. nickel [ppb]	Part. nickel [ppb]	Sol. iron [ppb]	Boron [ppm]
0.00	0.00	2.15	0.1923	2.0410	1.7949	1362
3.91	0.15	2.15	0.1923	2.0433	1.7951	1362
13.03	0.50	2.15	0.1970	2.1020	1.8087	1351
26.07	1.00	2.15	0.1979	2.1594	1.7875	1354
52.13	2.00	2.15	0.3360	3.8653	3.1632	1374
78.20	3.00	2.15	0.1903	2.6188	1.7331	1371
104.26	4.00	2.15	0.1858	2.5226	1.6993	1345
156.39	6.00	2.15	0.1866	2.4407	1.6733	1244
208.52	8.00	2.15	0.1843	2.3697	1.6825	1101
260.65	10.00	2.15	0.1815	2.3517	1.7212	934
312.79	12.00	2.15	0.1789	2.3665	1.7917	753
364.92	14.00	2.15	0.1771	2.4132	1.9104	564
417.05	16.00	2.00	0.1758	2.4835	2.0566	372
501.55	19.24	0.85	0.1752	2.6263	1.9490	65

Table 9. Geometry of the Seabrook assembly model

Parameter	Value	Units
Assembly pitch	21.5	cm
Active length	365.761	cm
Pellet radius	0.4096	cm
Pellet rings	10	—
Gap conductance	5,678.3	W/m^2-K
Clad inner radius	0.418	cm
Clad outer radius	0.475	cm
Rod pitch	1.26	cm
END grid loss coefficient	0.9070	—
MID grid loss coefficient	0.9065	—
END grid blockage ratio	0.83	—
MID grid blockage ratio	0.85	—

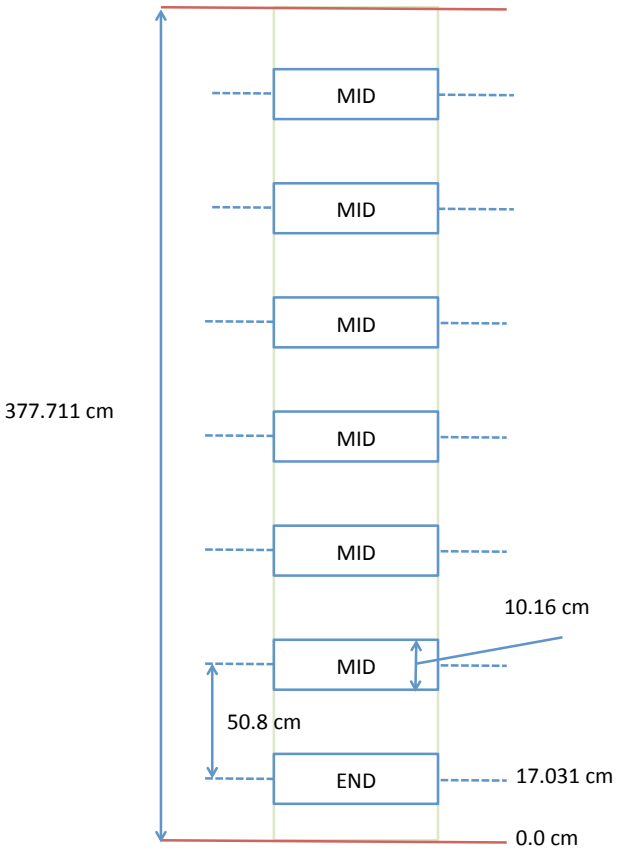

Figure 19. Grid placement in Seabrook model.

Substituting the heat rate, $\dot{q}$, with 3411 MW and the enthalpy rise, Δh, with 193.3 $\frac{\mathrm{J}}{\mathrm{g}}$ leads to a mass flow rate of 17 646.1 $\frac{\mathrm{kg}}{\mathrm{s}}$. We multiply this by 94.2 % to obtain the flow through the active portion of the core; this results in a total core flow rate of 16 622.7 $\frac{\mathrm{kg}}{\mathrm{s}}$. This value converts to 131.93 Mlbm/h, which compares favorably with the typical 4-loop PWR mass flow rate of 131.68 Mlbm/h given in Table 6. This is scaled to a single assembly by assuming uniform flow at the inlet and dividing by 193. This leads to a single assembly inlet flow rate of 86.13 $\frac{\mathrm{kg}}{\mathrm{s}}$.

8.2.2 Results

Running the full 14-state coupled CTF/MAMBA1D simulation takes about 90–100 minutes on the Natasha Fissile4 cluster. The case is run in serial, as it is a single-assembly case. Figure 20 shows the axial CRUD thickness profile for the failed rod in the G69 assembly. The steaming rate is included in the plot (red line) to show how it coincides with the CRUD deposit locations. The CRUD thickness profile is for the end of the cycle (i.e., 501 days). Figure 21 shows the radial distribution of CRUD in the assembly for the most CRUDed axial location of the assembly at this time. The location of the failed rod in the assembly is highlighted in blue.

The effect of the grids is observed in Figure 20 as a result of their effect on suppressing rod downstream surface temperatures (and thus boiling) through enhanced turbulence. CRUD thickness drops downstream of the grid and then quickly rises to reach a maximum just prior to the next grid. Maximum CRUD deposits are observed in the second-to-top grid span. Downstream of this, the power drops and boiling decreases. Figure 21 shows that the failed rod does not experience the thickest CRUD deposits. The thickest CRUD deposits are on the central rods residing next to the instrument tube. However, they have only about 2 µm of additional CRUD compared with the rod that experiences failure.

Ultimately, we can see that CTF/MAMBA1D is significantly underpredicting the CRUD growth experienced in the Seabrook Cycle 5 core. A CRUD scrape performed on the core produced an intact CRUD flake that measured 85 µm in thickness (see Figure 23) [12]. The predicted CRUD thicknesses in the CTF/MAMBA1D simulation are about half of this value.

Figure 22 shows the axial distribution of CRUD mass density on Rod M14 at the end of the cycle. The total mass of CRUD deposited on Assembly G69 at the end of the cycle is 0.61 kg; maximum deposits are experienced at the end of the cycle. The boron absorbed in the CRUD layer peaks at 261 days at a value of 1.57×10^{-4} kg. CRUD boron mass begins to deplete after this because of the reduction in the boron coolant. Boron mass at the end of the cycle is 6.65×10^{-5} kg.

Rod L7 fails in Assembly G70. The axial CRUD thickness profile looks similar to that obtained for Rod M14 in Assembly G69. Figure 24 shows this profile. Figure 25 shows the lateral CRUD thickness distribution at the most heavily CRUDed axial location. Both figures are taken from the end of the 501 day cycle.

The CRUD layer boron mass also reaches a maximum at 261 days in the cycle. The maximum value is 1.59×10^{-4} kg. the maximum CRUD mass occurs at the end of the cycle. The total mass of deposits on assembly G70 is 0.62 kg.

Although the CRUD deposits are considerably less than the flake obtained from Seabrook, it is important to mention that the flake represents a small location on the fuel rod, while the results obtained by MAMBA1D are for a much larger surface of the fuel rod. Furthermore, the four surfaces of the fuel rod are averaged over the circumference of the rod. It is possible that the flake came from a particularly thick peak in the CRUD.

Note that the power distribution is not completely accurate because of the absence of the spacer grids in the neutronics model; however, it is unclear how large an impact this would have on localized boiling rates outside of the grid region. It would be useful if we could obtain a more detailed specification for the Seabrook core, as several assumptions were required because of limited geometric information on the problem.

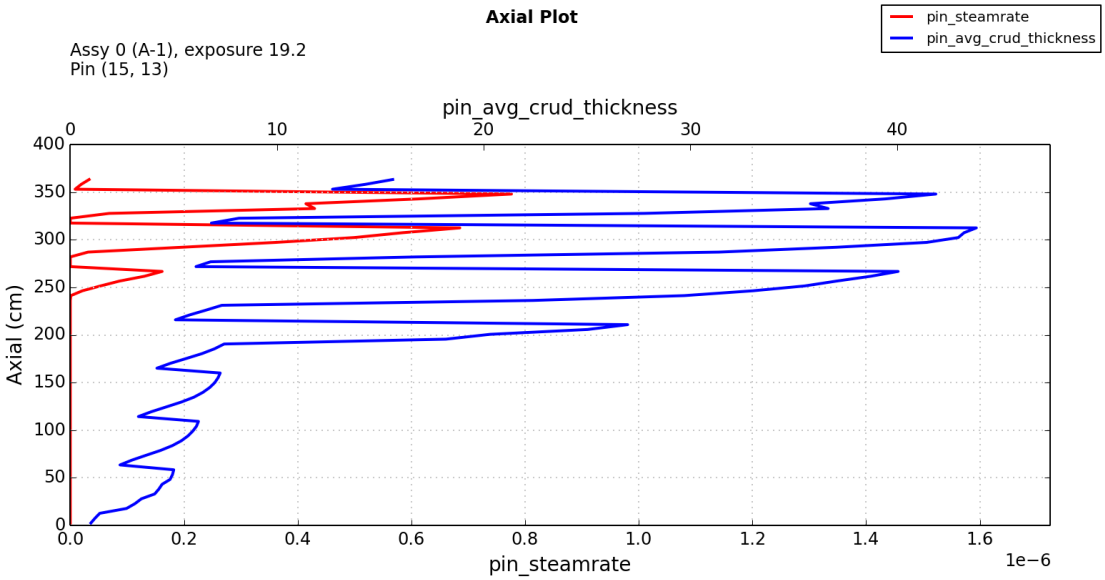

Figure 20. Axial CRUD thickness in microns (blue line) and steaming rate in $\frac{\text{kg}}{\text{s}}$ (red line) distribution on Rod M14 (failed rod) in Assembly G69 at 501 days.

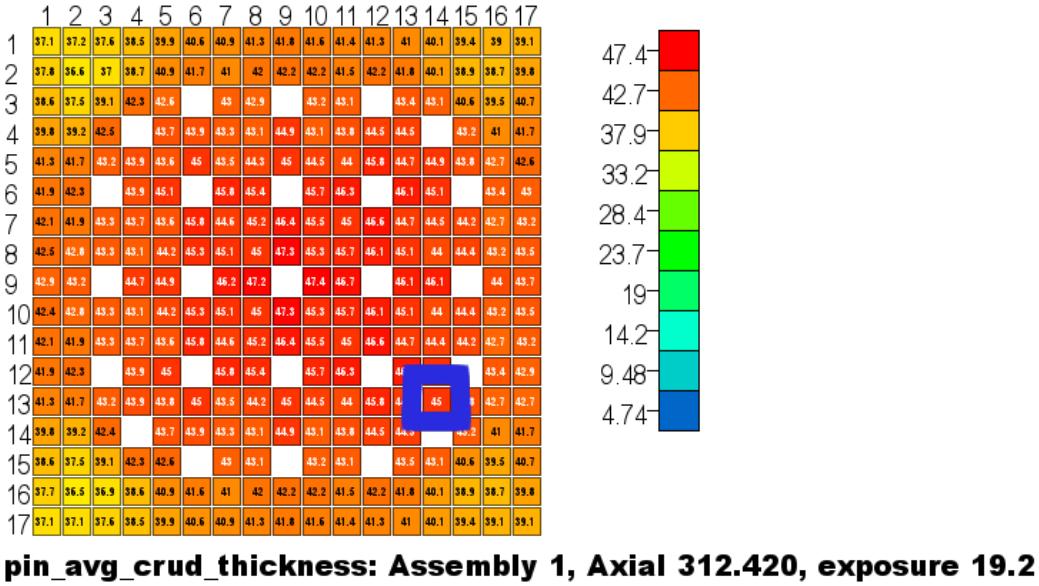

Figure 21. CRUD thickness on rods in G69 at 501 days and at axial location with thickest CRUD deposits (Rod M14 highlighted in blue).

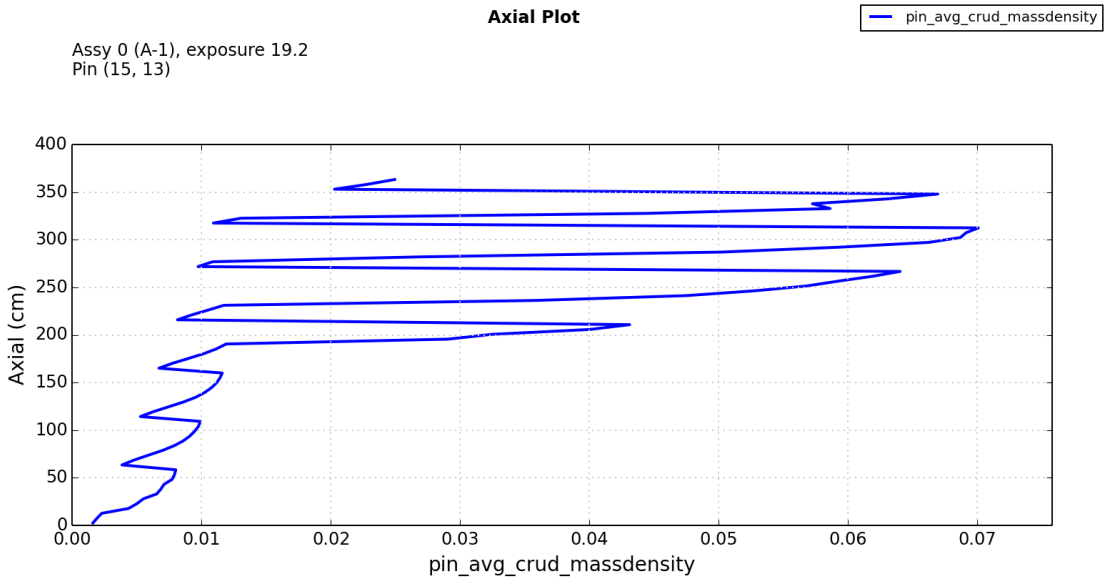

Figure 22. CRUD mass density along the axial length of Rod M14 at the end of cycle.

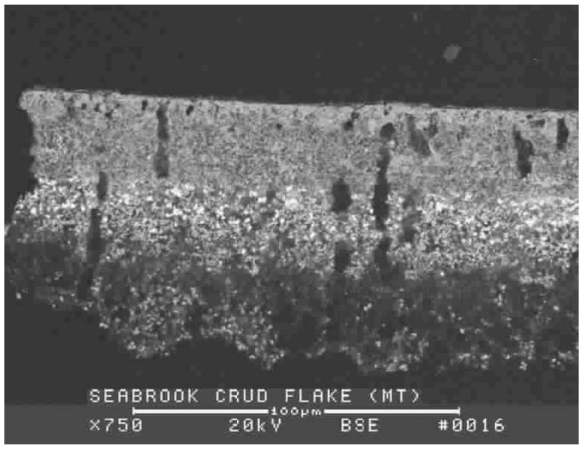

Figure 23. Intact CRUD flake obtained from CRUD scrape (measures 85 µm in thickness).

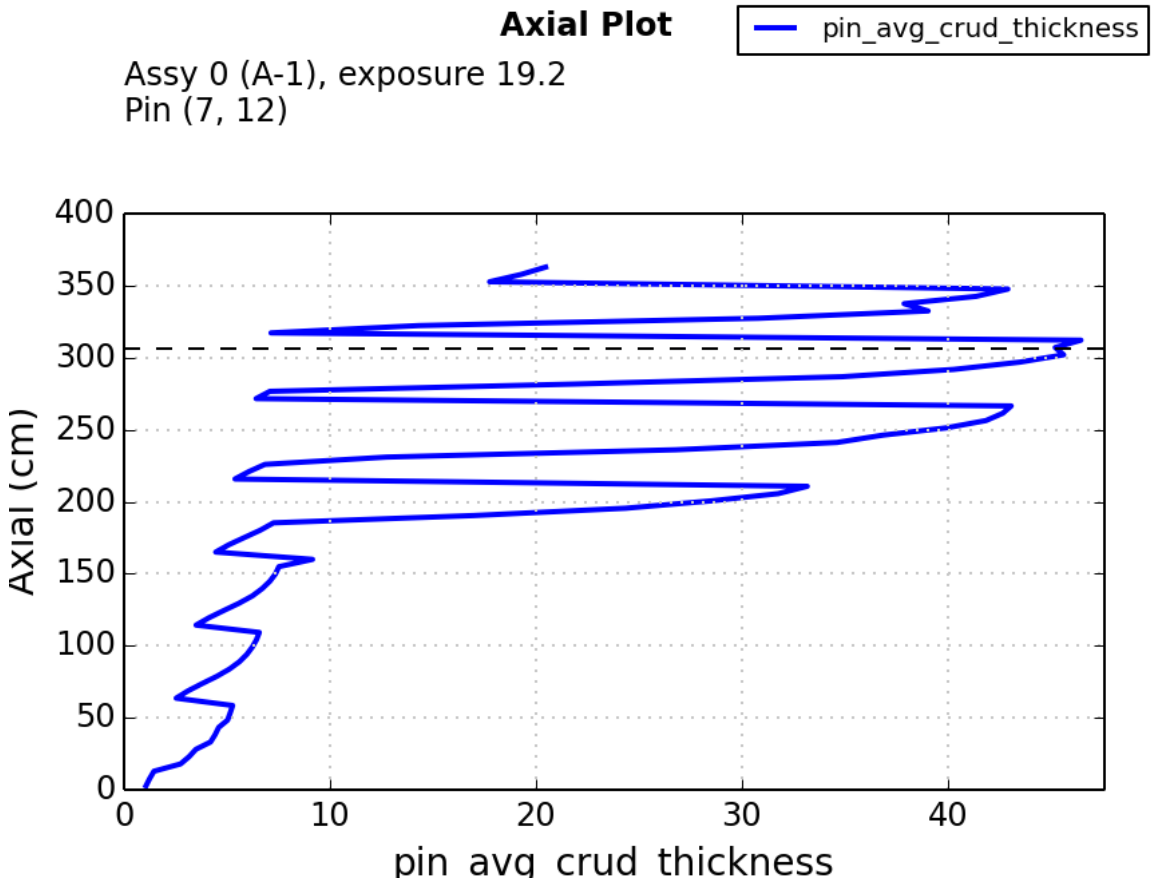

Figure 24. Axial CRUD thickness (microns) distribution on Rod L7 (failed rod) in Assembly G70 at 501 days.

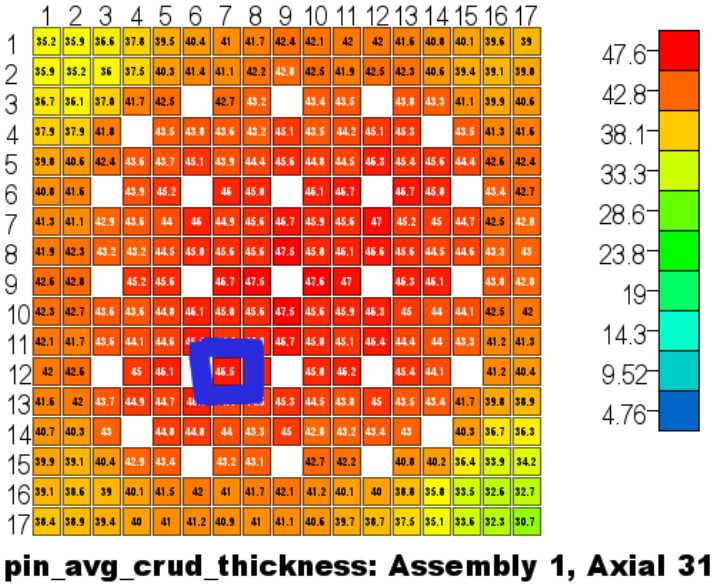

Figure 25. CRUD thickness on rods in G70 at 501 days and at axial location with thickest CRUD deposits (Rod L7 highlighted in blue).

9 Conclusion

This milestone results in a new coupled subchannel (CTF) and CRUD (MAMBA1D) modeling capability in VERA-CS. Completion of this milestone required completing several tasks, including completing follow-on tasks from the previous milestone, integrating MAMBA1D into the TriBITs build and test system, linking CTF to MAMBA1D, considering how the erosion and boiling models may be handled, expanding the HDF5 output with new CRUD data, and testing the new features.

The erosion model presents a challenge because it requires TKE as an input, which is not a value calculated by CTF. This is solved by implementing a conversion from the CTF-calculated rod shear stress to an approximation of TKE. While a physics-based model was found in the literature, ultimately, a simple method was implemented that ensures that an average TKE of 0.1 $\frac{\text{J}}{\text{kg}}$ is delivered to MAMBA1D, which is the value it expects in order to produce a suitable CRUD erosion rate.

The boiling model also presents a challenge because each of the codes uses its own rod boiling models. Since the MAMBA1D boiling model models chimney boiling and the CTF model represents surface boiling, it was decided that both should continue to be used in the solution. The assumption is made that all CRUD chimney vapor generation condenses before entering the CTF solution space, resulting in implicit heat transfer from the CRUD region to the CTF solution space region. It is possible that the MAMBA1D boiling model has been tuned to include effects of surface boiling, which would result in double-counting of rod surface heat transfer due to boiling; however, a sensitivity analysis shows that CTF-predicted surface boiling is about 4 orders of magnitude smaller than MAMBA1D chimney boiling, making it an insignificant contributor to rod-to-fluid heat transfer.

A simulation of Seabrook Cycle 5 was performed to demonstrate the feature. Although the demonstration was successful, the predicted CRUD thicknesses appear to be somewhat thin compared with the actual CRUD scrape measurements, which are twice as thick as CTF/MAMBA1D predictions.

Future work includes performing further analysis of the suitability of the chosen coupling algorithm (i.e.,whether it is safe to neglect the internal chimney boiling heat and mass transfer effects). Additionally, the Seabrook case should be further investigated to determine the cause of the CRUD thickness underprediction. Finally, additional milestones will seek to expand the coupling to a three-way approach that considers neutronics, T/H, and CRUD.

References

[1] R. Salko et al. *Development of CTF Capability for Modeling Reactor Operating Cycles with Crud Growth*. Tech. rep. CASL-U-2014-0188-000. Consortium for Advanced Simulation of Light Water Reactors, Oct. 2014.

[2] R. Salko et al. "Completion Memo for Milestone L3:PHI.CTF.P10.02". Memo documenting milestone completion.

[3] B. Collins. *CRUD Modeling in MPACT*. Tech. rep. CASL-U-2015-0166-000. Consortium for Advanced Simulation of Light Water Reactors, 2015.

[4] B. Collins, R. Salko, and S. Stimpson. *VERA-CS with CIPS Modeling Capability*. Tech. rep. CASL-I-2015-0285-000. Consortium for Advanced Simulation of Light Water Reactors, 2015.

[5] J. Secker et al. *Qualify a Core-Wide PWR CIPS Capability that Includes an Initial Corrosion Product Treatment*. Tech. rep. CASL-I-2015-0318-000. Consortium for Advanced Simulation of Light Water Reactors, 2015.

[6] P. Bradshaw. "The turbulence structure of equilibrium boundary layers". In *J. Fluid Mech.* 29 (1967), pp. 625–645.

[7] P.T. Harsha and S.C. Lee. "Correlation between turbulent shear stress and turbulent kinetic energy". In *AIAA Journal* 8 (1970), pp. 1508–1510.

[8] P. Bradshaw and G.E. Hellens. *The N.P.L. 59 in. by 9 in. Boundary-Layer Tunnel*. Tech. rep. 3437. Aeronautical Research Council, 1964.

[9] G.B. Wallis. *One-Dimensional Two-Phase Flow*. McGraw-Hill, 1969.

[10] G. Wang, A. Byers, and M. Young. *Simulated Fuel Crud Thermal Conductivity Measurements Under Pressurized Water Reactor Conditions*. Tech. rep. 1022896. Electric Power Research Institute, 2011.

[11] A. Godfrey. *VERA Core Physics Benchmark Progression Problem Specifications*. Tech. rep. CASL-U-2012-003. Revision 3. Consortium for Advanced Simulation of Light Water Reactors, Mar. 2014.

[12] J. Secker et al. *Coupled COBRA-TF/MAMBA2D Multiphysics Models for Seabrook 1 Cycle 5 Assembly G70 5x5 Rod Array and Assembly G64 7x7 Rod Array*. Tech. rep. CASL-I-2013-0191-001. Consortium for Advanced Simulation of Light Water Reactors, 2013.